

**Axion field and the quark nugget's formation at the QCD phase transition**

Xunyu Liang and Ariel Zhitnitsky

*Department of Physics and Astronomy, University of British Columbia, Vancouver V6T 1Z1, Canada*

(Received 21 June 2016; published 3 October 2016)

We study a testable dark-matter (DM) model outside of the standard weakly interacting massive particle paradigm in which the observed ratio  $\Omega_{\text{dark}} \approx \Omega_{\text{visible}}$  for visible and dark-matter densities finds its natural explanation as a result of their common QCD origin when both types of matter (DM and visible) are formed at the QCD phase transition and both are proportional to  $\Lambda_{\text{QCD}}$ . Instead of the conventional “baryogenesis” mechanism, we advocate a paradigm when the “baryogenesis” is actually a charge separation process which always occurs in the presence of the  $CP$  odd axion field  $a(x)$ . In this scenario, the global baryon number of the Universe remains zero, while the unobserved antibaryon charge is hidden in the form of heavy nuggets, similar to Witten’s strangelets and compromise the DM of the Universe. In the present work, we study in great detail a possible formation mechanism of such macroscopically large heavy objects. We argue that the nuggets will be inevitably produced during the QCD phase transition as a result of Kibble-Zurek mechanism on formation of the topological defects during a phase transition. Relevant topological defects in our scenario are the closed bubbles made of the  $N_{\text{DW}} = 1$  axion domain walls. These bubbles, in general, accrete the baryon (or antibaryon) charge, which eventually results in the formation of the nuggets and antinuggets carrying a huge baryon (antibaryon) charge. A typical size and the baryon charge of these macroscopically large objects are mainly determined by the axion mass  $m_a$ . However, the main consequence of the model,  $\Omega_{\text{dark}} \approx \Omega_{\text{visible}}$ , is insensitive to the axion mass which may assume any value within the observationally allowed window  $10^{-6} \text{ eV} \lesssim m_a \lesssim 10^{-3} \text{ eV}$ . We also estimate the baryon-to-entropy ratio  $\eta \equiv n_B/n_\gamma \sim 10^{-10}$  within this scenario. Finally, we comment on implications of these results to the axion search experiments, including the microwave cavity and the Orpheus experiments.

DOI: [10.1103/PhysRevD.94.083502](https://doi.org/10.1103/PhysRevD.94.083502)**I. INTRODUCTION**

The origin of the observed asymmetry between matter and antimatter is one of the largest open questions in cosmology. The nature of the dark matter (DM) is another open question in cosmology. In this paper, we advocate an idea that these two, apparently unrelated, problems are in fact two sides of the same coin. Furthermore, both mysterious effects are originated at one and the same cosmological epoch from one and the same QCD physics. Normally, it is assumed that the majority of dark matter is represented by a new fundamental field coupled only weakly to the standard model particles; these models may then be tuned to match the observed dark-matter properties. We take a different perspective and consider the possibility that the dark matter is in fact composed of well-known quarks and antiquarks but in a new high-density phase, similar to Witten’s strangelets; see the original work [1] and some related studies [2].

There are few new crucial elements in proposal [3,4], in comparison with previous studies [1,2]. First of all, the nuggets could be made of matter as well as antimatter in our framework as a result of the separation of charges; see a few comments below. Second, the stability of the DM nuggets is provided by the axion domain walls with extra pressure, in contrast with original studies when stability is assumed to be achieved even in vacuum, at zero external pressure.

Finally, an overall coherent baryon asymmetry in the entire Universe is a result of the strong  $CP$  violation due to the fundamental  $\theta$  parameter in QCD which is assumed to be nonzero at the beginning of the QCD phase transition. This source of strong  $CP$  violation is no longer available at the present epoch as a result of the axion dynamics; see the original papers [5–7] and recent reviews [8–15] on the subject. We highlight the basic ideas of this framework in the present Introduction, while we elaborate on these new crucial elements in details in Sec. III.

It is generally assumed that the Universe began in a symmetric state with zero global baryonic charge and later (through some baryon number-violating process) evolved into a state with a net positive baryon number. As an alternative to this scenario, we advocate a model in which “baryogenesis” is actually a charge separation process in which the global baryon number of the Universe remains zero. In this model, the unobserved antibaryons come to comprise the dark matter. A connection between dark matter and baryogenesis is made particularly compelling by the similar energy densities of the visible and dark matter with  $\Omega_{\text{dark}} \approx 5 \cdot \Omega_{\text{visible}}$ . If these processes are not fundamentally related, the two components could exist at vastly different scales.

In the model [3,4], baryogenesis occurs at the QCD phase transition. Both quarks and antiquarks are thermally

abundant in the primordial plasma, but in addition to forming conventional baryons, some fraction of them is bound into heavy nuggets of quark matter in a color superconducting phase. Nuggets of both matter and anti-matter are formed as a result of the dynamics of the axion domain walls as originally proposed in Refs. [3,4]. A number of very hard dynamical questions in strongly coupled QCD which are related to the nuggets's formation have not been studied in any details in the original papers. The main goal of the present work is to make the first step in the direction to address these hard questions.

If the fundamental  $\theta$  parameter were identically zero at the QCD phase transition in the early Universe, an equal number of nuggets made of matter and antimatter would be formed. It would result in the vanishing of the visible baryon density at the present epoch. However, the fundamental  $CP$ -violating processes associated with the  $\theta$  term in QCD (which is assumed to be small but still nonzero at the very beginning of the QCD phase transition) result in the preferential formation of antinuggets over the nuggets. This preference is essentially determined by the dynamics of coherent axion field  $\theta(x)$  at the initial stage of the nugget's formation. The resulting asymmetry is not sensitive to a small magnitude of the axion field  $\theta(x)$  at the QCD phase transition as long as it remains coherent on the scale of the Universe; see Sec. VII for details.

The remaining antibaryons in the plasma then annihilate away, leaving only the baryons of which the antimatter counterparts are bound in the excess of antinuggets and thus unavailable to annihilate. All asymmetry effects are order of 1, irrespective of the magnitude of  $\theta(x)$  at the moment of formation. This is precisely the main reason of why the visible and dark-matter densities must be the same order of magnitude

$$\Omega_{\text{dark}} \approx \Omega_{\text{visible}} \quad (1)$$

as they are both proportional to the same fundamental  $\Lambda_{\text{QCD}}$  scale, and they both originated at the same QCD epoch. In particular, if one assumes that the nuggets and antinuggets saturate the dark-matter density, then the observed matter-to-dark-matter ratio  $\Omega_{\text{dark}} \approx 5 \cdot \Omega_{\text{visible}}$  corresponds to a specific proportion when the number of antinuggets is larger than number of nuggets by a factor of  $\sim 3/2$  at the end of the nugget's formation. This would result in a matter content with baryons, quark nuggets, and antiquark nuggets in an approximate ratio,

$$|B_{\text{visible}}| : |B_{\text{nuggets}}| : |B_{\text{antinuggets}}| \approx 1 : 2 : 3, \quad (2)$$

with no net baryonic charge. If these processes are not fundamentally related, the two components  $\Omega_{\text{dark}}$  and  $\Omega_{\text{visible}}$  could easily exist at vastly different scales.

Though the QCD phase diagram at  $\theta \neq 0$  as a function of  $T$  and  $\mu$  is basically unknown, it is well understood that  $\theta$  is

in fact the angular variable and therefore supports various types of the domain walls, including the so-called  $N_{DW} = 1$  domain walls when  $\theta$  interpolates between one and the same physical vacuum state  $\theta \rightarrow \theta + 2\pi$ . Furthermore, it is expected that the closed bubbles made of these  $N_{DW} = 1$  axion domain walls are also produced during the QCD phase transition with a typical wall tension  $\sigma_a \sim m_a^{-1}$  where  $m_a$  is the axion mass. Precisely this scale determines the size and the baryon charge of the nuggets; see Eqs. (3) and (4) below.

The collapse of these close bubbles is halted due to the Fermi pressure acting inside of the bubbles. The crucial element which stops the collapse of the bubbles from complete annihilation is the presence of the QCD substructure inside the axion domain wall. This substructure forms immediately after the QCD phase transition as discussed in Ref. [3]. The equilibrium of the obtained system has been analyzed in Ref. [3] for a specific axion domain wall tension within the observationally allowed window  $10^{-6} \text{ eV} \leq m_a \leq 10^{-3} \text{ eV}$  consistent with the recent constraints [8–15]. It has been also argued in Ref. [3] that the equilibrium is typically achieved when the Fermi pressure inside the nuggets falls into the region when the color superconductivity (CS) indeed sets in.<sup>1</sup>

The size and the baryon charge of the nuggets scale with the axion mass as follows:

$$\sigma_a \sim m_a^{-1}, \quad R \sim \sigma_a, \quad B \sim \sigma_a^3. \quad (3)$$

Therefore, when the axion mass  $m_a$  varies within the observationally allowed window  $10^{-6} \text{ eV} \lesssim m_a \lesssim 10^{-3} \text{ eV}$ , the nuggets parameters also vary as

$$10^{-6} \text{ cm} \lesssim R \lesssim 10^{-3} \text{ cm}, \quad 10^{23} \lesssim B \lesssim 10^{32}, \quad (4)$$

where the lowest axion mass  $m_a \approx 10^{-6} \text{ eV}$  approximately<sup>2</sup> corresponds to the largest possible nuggets with  $\langle B \rangle \approx 10^{32}$ . Variation of the axion mass by 3 orders of magnitude results in variation of the nugget's baryon charge by 9 orders of magnitude according to relation (3). The corresponding allowed region is essentially unconstrained by present experiments; see details in Sec. II below.

<sup>1</sup>There is no requirement on the first-order phase transition (in contrast with original proposal [1]) for the bubble formation in this framework because the  $N_{DW} = 1$  axion domain walls are formed irrespective of the order of the phase transition. Needless to say, the phase diagram in general and the order of the phase transition in particular at  $\theta \neq 0$  are still unknown because of the longstanding ‘‘sign problem’’ in the QCD lattice simulations at  $\theta \neq 0$ ; see a few comments and related references in the Conclusion.

<sup>2</sup>There is no one-to-one correspondence between the axion mass  $m_a$  and the baryon charge of the nuggets  $B$  because for each given  $m_a$  there is an extended window of stable solutions describing different nuggets' sizes [3].

The fact that the CS may be realized in nature in the cores of neutron stars has been known for some time [16,17]. A new element which was advocated in proposal [3] is that a similar dense environment can be realized in nature due to the axion domain wall pressure playing the role of a “squeezer,” similar to the gravity pressure in the neutron star physics.

Another fundamental ratio (along with  $\Omega_{\text{dark}} \approx \Omega_{\text{visible}}$  discussed above) is the baryon-to-entropy ratio at the present time,

$$\eta \equiv \frac{n_B - n_{\bar{B}}}{n_\gamma} \approx \frac{n_B}{n_\gamma} \sim 10^{-10}. \quad (5)$$

If the nuggets were not present after the phase transition, the conventional baryons and antibaryons would continue to annihilate each other until the temperature reaches  $T \approx 22$  MeV when density would be 9 orders of magnitude smaller than observed (5). This annihilation catastrophe is normally thought to be resolved as a result of baryogenesis as formulated by Sakharov [18]; see also review [19]. In this framework, the ratio (5) is highly sensitive to many specific details of the models such as the spectrum of the system in general and the coupling constants and the strength of  $CP$  violation in particular; see, e.g., review [19].

In our proposal (in contrast with conventional frameworks on baryogenesis), this ratio is determined by a single parameter with a typical QCD scale, the formation temperature  $T_{\text{form}}$ . This temperature is defined by a moment in evolution of the Universe when the nuggets and antinuggets basically have completed their formation and not much annihilation would occur at lower temperatures  $T \leq T_{\text{form}}$ . The exact magnitude of temperature  $T_{\text{form}} \sim \Lambda_{\text{QCD}}$  in our proposal is determined by many factors: transmission/reflection coefficients, evolution of the nuggets, expansion of the Universe, cooling rates, evaporation rates, viscosity of the environment, the dynamics of the axion domain wall network, etc. All these effects, in general, equally contribute to  $T_{\text{form}}$  at the QCD scale. Technically, the corresponding effects are hard to compute from the first principles as even basic properties of the QCD phase diagram at nonzero  $\theta \neq 0$  are still unknown.<sup>3</sup> We plot three different conjectured cooling paths on Fig. 1.

<sup>3</sup>The basic consequences (1) as well as (5) of this proposal are largely insensitive to the absolute value of the initial magnitude of the  $\theta$  parameter. In other words, a fine-tuning of the initial  $\theta$  parameter is not required in this mechanism. The same comment (on the “insensitivity” of the initial conditions) also applies to the efficiency of the nugget’s formation. This is because the baryon density at the present time is 10 orders of magnitude lower than the particle density at the QCD phase transition epoch according to the observations (5). Therefore, even a sufficiently low efficiency of the nugget’s formation (still larger than  $10^{-7}$ ; see the estimates in Sec. VII C) cannot drastically modify the generic relations (1), (5) due to a long evolution which eventually washes out any sensitivity to the initial conditions. The only crucial parameter which determines the final outcome (1), (5) is the formation temperature  $T_{\text{form}}$  as estimated below.

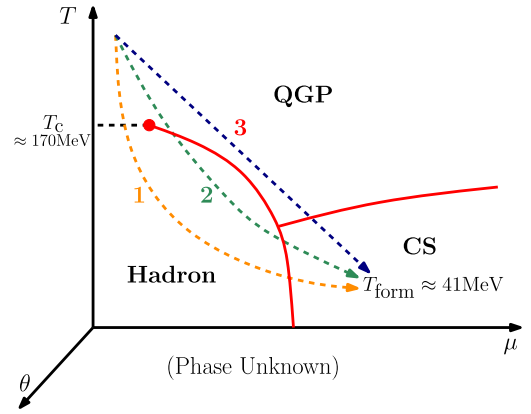


FIG. 1. The conjectured phase diagram. Possible cooling paths are denoted as path 1, 2, or 3. The phase diagram is in fact much more complicated as the dependence on the third essential parameter, the  $\theta$ , is not shown as it is largely unknown. Therefore, the paths should be thought as lines in three-dimensional parametrical space, not as lines on the two-dimensional  $(\mu, T)$  slice at  $\theta = 0$  as shown on the present plot. It is assumed that the final destination after the nuggets are formed is the region with  $T_{\text{form}} \approx 41$  MeV,  $\mu > \mu_c$  and  $\theta \approx 0$ , corresponding to the presently observed ratio (5); see the text for the details.

However, the estimate of  $T_{\text{form}}$  up to factor 2 is quite a simple exercise as  $T_{\text{form}}$  must be proportional to the gap  $\Delta \sim 100$  MeV when the CS phase sets in inside the nuggets. The observed ratio (5) corresponds to  $T_{\text{form}} \approx 40$  MeV; see Ref. [4] for details. This temperature indeed represents a typical QCD scale, slightly below the critical temperature  $T_{\text{CS}} \approx 0.6\Delta \approx 60$  MeV, according to standard estimates on color superconductivity; see reviews [16,17].

Unlike conventional dark-matter candidates, such as weakly interacting massive particles (WIMPs), the dark-matter/antimatter nuggets are strongly interacting but macroscopically large. They do not contradict any of the many known observational constraints on dark matter or antimatter for three main reasons [20]:

- (i) They carry a huge (anti)baryon charge  $|B| \gtrsim 10^{25}$  and so have an extremely tiny number density.
- (ii) The nuggets have nuclear densities, so their effective interaction is small,  $\sigma/M \sim 10^{-10}$  cm<sup>2</sup>/g, well below the typical astrophysical and cosmological limits which are on the order of  $\sigma/M < 1$  cm<sup>2</sup>/g.
- (iii) They have a large binding energy  $\sim \Delta$ , such that the baryon charge in the nuggets is not available to participate in big bang nucleosynthesis at  $T \approx 1$  MeV.

To reiterate, the weakness of the visible-dark matter interaction is achieved in this model due to the small geometrical parameter  $\sigma/M \sim B^{-1/3}$  rather than due to a weak coupling of a new fundamental field with standard model particles. In other words, this small effective interaction  $\sim \sigma/M \sim B^{-1/3}$  replaces a conventional requirement of sufficiently weak interactions of the visible matter with WIMPs.

As we already mentioned, this model when DM is represented by quark and antiquark nuggets is consistent with fundamental astrophysical constraints as highlighted above. Furthermore, there is a number of frequency bands where some excess of emission was observed but not explained by conventional astrophysical sources. Our comment here is that this model may explain some portion, or even the entire excess, of the observed radiation in these frequency bands. This phenomenological part of the proposal is the key ingredient in our advocacy of the model and may play a very important role for the interpretation of the present and future observations. Therefore, we devote the Sec. II to reviewing the original results [21–30] where predictions of the model have been confronted with the observations in specific frequency bands covering more than 11 orders of magnitude, from radio frequency with  $\omega \sim 10^{-4}$  eV to  $\gamma$  rays with  $\omega \sim 10$  MeV. We also mention in Sec. II some interesting results [31–35], which are presently perfectly consistent with the model. However, in the future, the same studies with modest improvements will provide a powerful test of the viability of the quark nugget dark-matter model.

One should emphasize here that the corresponding analysis [21–30] is determined by conventional physics, and as such all effects are calculable from the first principles. In other words, the model contains no tuneable fundamental parameters, except for a single mean baryon number of a nugget  $\langle B \rangle \sim 10^{25}$  which enters all the computations [21–30] as a single normalization factor. At the same time, the crucial assumptions of the model, such as specific mechanisms on the baryon charge separation, dynamics of the nugget formation, etc., have never been explored in our previous studies.

We believe that the phenomenological success [21–30] of the model warrants further theoretical studies of this framework, in spite of its naively counterintuitive nature. Therefore, the present work should be considered as the first step in this direction where we attempt to develop the theoretical framework to address (and hopefully answer) some of the hardest questions about a possible mechanism for the nugget’s formation during the QCD phase transition in the strongly coupled regime when even the phase diagram at  $\theta \neq 0$  as a function of the chemical potential  $\mu$  and temperature  $T$  is still unknown; see footnote 1.

The structure of this work is as follows. In Sec. II, we briefly review the observational constraints on the model. In Sec. III, we highlight the basic assumptions and ingredients of this framework, while in Secs. IV and V, we present some analytical estimates which strongly substantiate the idea that such heavy objects indeed can be formed and survive until the present epoch during the QCD phase transition in the early Universe. Section VI as well as Appendixes A and B are devoted to a number of technical details which support our basic claim.

In Sec. VII, we argue that there will be the preferential formation of one species of nuggets over another. This preference is determined by the dynamics of the axion field  $\theta(x)$  which itself is correlated on the scales of the Universe at the beginning of the nugget’s formation. Finally, in Sec. VIII we comment on implications of our studies to direct axion search experiments.

To conclude this long Introduction, the nuggets in our framework play the *dual* role: they serve as the DM candidates, and they also explain the observed asymmetry between matter and antimatter. These two crucial elements of the proposal lead to a very generic consequence of the entire framework expressed by Eq. (1). This basic generic result is not very sensitive to any specific details of the model but rather entirely determined by two fundamental ingredients of the framework:

- (i) the contribution to  $\Omega$  for both types of matter (visible and dark) are proportional to one and the same fundamental scale  $\sim \Lambda_{\text{QCD}}$ ;
- (ii) the preferential formation of one species of nuggets over another is correlated on huge cosmological scales where  $CP$ -violating axion phase  $\theta(x)$  remains coherent just a moment before the QCD phase transition.

The readers interested in the cosmological consequences, rather than in technical computational details, may directly jump to Sec. III where we formulate the basics ingredients of the proposal, to Sec. VII B where we explain the main model-independent consequence (1) of this framework, and to Sec. VIII where we make a few comments on implications to other axion search experiments, including microwave cavity [8–10,13] and the Orpheus experiments [14].

## II. QUARK (ANTI)NUGGET DM CONFRONTING THE OBSERVATIONS

While the observable consequences of this model are on average strongly suppressed by the low number density of the quark nuggets  $\sim B^{-1/3}$  as explained above, the interaction of these objects with the visible matter of the Galaxy will necessarily produce observable effects. Any such consequences will be largest where the densities of both visible and dark matter are largest such as in the core of the Galaxy or the early Universe. In other words, the nuggets behave as a conventional cold DM in the environment where the density of the visible matter is small, while they become interacting and emit radiation objects (i.e., effectively become visible matter) when they are placed in the environment with sufficiently large density.

The relevant phenomenological features of the resulting nuggets are determined by properties of the so-called electrosphere as discussed in Refs. [21–30]. These properties are, in principle, calculable from first principles using only the well-established and known properties of QCD and QED. As such, the model contains no tuneable fundamental parameters, except for a single mean baryon number

$\langle B \rangle$  which itself is determined by the axion mass  $m_a$  as we already mentioned.

A comparison between emissions with drastically different frequencies from the center of the Galaxy is possible because the rate of annihilation events (between visible matter and antimatter DM nuggets) is proportional to the product of the local visible and DM distributions at the annihilation site. The observed fluxes for different emissions thus depend on one and the same line-of-sight integral

$$\Phi \sim R^2 \int d\Omega dl [n_{\text{visible}}(l) \cdot n_{\text{DM}}(l)], \quad (6)$$

where  $R \sim B^{1/3}$  is a typical size of the nugget which determines the effective cross section of interaction between DM and visible matter. As  $n_{\text{DM}} \sim B^{-1}$ , the effective interaction is strongly suppressed  $\sim B^{-1/3}$  as we already mentioned in the Introduction. The parameter  $\langle B \rangle \sim 10^{25}$  was fixed in this proposal by assuming that this mechanism saturates the observed 511 keV line [21,22], which resulted from annihilation of the electrons from visible matter and positrons from antinuggets. It has been also assumed that the observed dark-matter density is saturated by the nuggets and antinuggets. It corresponds to an average baryon charge  $\langle B \rangle \sim 10^{25}$  for typical density distributions  $n_{\text{visible}}(r)$ ,  $n_{\text{DM}}(r)$  entering (6). Other emissions from different bands are expressed in terms of the same integral (6), and therefore the relative intensities are completely determined by the internal structure of the nuggets which is described by conventional nuclear physics and basic QED. We present a short overview of these results below.

Some galactic electrons are able to penetrate to a sufficiently large depth of the antinuggets. These events no longer produce the characteristic positronium decay spectrum (511 keV line with a typical width of order  $\sim$ few keV accompanied by the conventional continuum due to  $3\gamma$  decay) but a direct nonresonance  $e^-e^+ \rightarrow 2\gamma$  emission spectrum. The transition between the resonance positronium decays and nonresonance regime is determined by conventional physics and allows us to compute the strength and spectrum of the MeV-scale emissions relative to that of the 511 keV line [23,24]. Observations by the COMPTEL satellite indeed show some excess above the galactic background consistent with our estimates.

Galactic protons incident on the antinugget will penetrate some distance into the quark matter before annihilating into hadronic jets. This process results in the emission of bremsstrahlung photons at x-ray energies [25]. Observations by the CHANDRA observatory apparently indicate an excess in x-ray emissions from the Galactic center.

Hadronic jets produced deeper in the nugget or emitted in the downward direction will be completely absorbed. They eventually emit thermal photons with radio

frequencies [26,27]. Again, the relative scales of these emissions may be estimated and are found to be in agreement with observations.

These apparent excess emission sources have been cited as possible support for a number of dark-matter models as well as other exotic astrophysical phenomenon. At present, however, they remain open matters for investigation and, given the uncertainties in the galactic spectrum and the wide variety of proposed explanations, are unlikely to provide clear evidence in the near future. Therefore, it would be highly desirable if some direct detection of such objects is found, similar to direct searches of the WIMPs.

While direct searches for WIMPs require large sensitivity, a search for very massive dark matter nuggets requires large area detectors. If the dark matter consists of quark nuggets at the  $B \sim 10^{25}$  scale, they will have a flux of

$$\frac{dN}{dAdt} = nv \approx \left( \frac{10^{25}}{B} \right) \text{ km}^{-2} \text{ yr}^{-1}. \quad (7)$$

Though this flux is far below the sensitivity of conventional dark matter searches, it is similar to the flux of cosmic rays near the Greisen Zatsepin Kuzmin (GZK) limit. As such, present and future experiments investigating ultrahigh energy cosmic rays may also serve as search platforms for dark matter of this type.

It has been suggested that large-scale cosmic-ray detectors may be capable of observing quark (anti)nuggets passing through the Earth's atmosphere either through the extensive air shower such an event would trigger [28] or through the geosynchrotron emission generated by the large number of secondary particles [29]; see also Ref. [30] for review.

It has also been estimated in Ref. [31] that, based on Apollo data, nuggets of mass from  $\sim 10$  kg to 1 ton (corresponding to  $B \sim 10^{28-30}$ ) must account for less than an order of magnitude of the local dark matter. While our preferred range of  $B \sim 10^{25}$  is somewhat smaller and is not excluded by Ref. [31], we still believe that  $B \geq 10^{28}$  is not completely excluded by the Apollo data, as the corresponding constraints are based on specific model-dependent assumptions about the nugget mass distribution.

It has also been suggested that the ANITA experiment may be sensitive to the radio band thermal emission generated by these objects as they pass through the Antarctic ice [32]. These experiments may thus be capable of adding direct detection capability to the indirect evidence discussed above; see Fig. 2 taken from Ref. [32], which reviews these constraints.

It has been also suggested recently [33] that the interactions of these (anti)nuggets with normal matter in the Earth and Sun will lead to annihilation and an associated neutrino flux. Furthermore, it has been claimed [33] that the antiquark nuggets cannot account for more than 20% of the dark-matter flux based on constraints for the neutrino flux

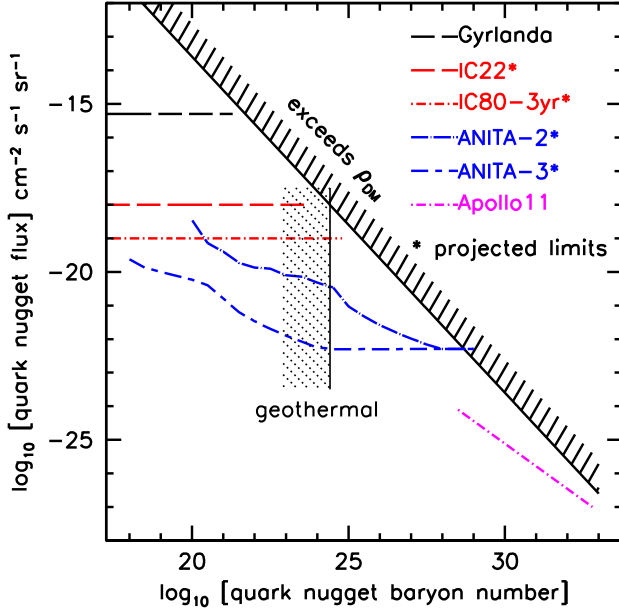


FIG. 2. Limits on quark nugget mass and fluxes based on current constraints, taken from Ref. [32]. Our preferable value  $\langle B \rangle \sim 10^{25}$  is translated to the axion mass  $m_a \approx 10^{-4}$  eV according to the scaling relation (3). The corresponding constraints expressed in terms of  $m_a$  have an important implication for the direct axion search experiments as discussed in Sec. VIII. Orpheus experiment “B” is designed to be sensitive exactly to this value of the axion mass  $m_a \approx 10^{-4}$  eV; see Fig. 3.

in the 20–50 MeV range where the sensitivity of the underground neutrino detectors such as SuperK have their highest signal-to-noise ratio.

However, the claim [33] was based on the assumption that the annihilation of visible baryons with antiquark nuggets generates the neutrino spectrum similar to conventional baryon-antibaryon annihilation spectrum when the large number of produced pions eventually decay to muons and consequently to highly energetic neutrinos in the 20–50 MeV energy range. Precisely these highly energetic neutrinos play the crucial role in analysis [33]. However, in most CS phases, the lightest pseudo-Goldstone mesons (the pions and kaons) have masses in the 5–20 MeV range [16,17], in huge contrast with hadronic confined phase where  $m_\pi \sim 140$  MeV. Therefore, such light pseudo-Goldstone mesons in the CS phase cannot produce highly energetic neutrinos in the 20–50 MeV energy range and thus are not subject to the SuperK constraints [35].

We conclude this brief overview on observational constraints of the model with the following remark. This model which has a single fundamental parameter (the mean baryon number of a nugget  $\langle B \rangle \sim 10^{25}$ , corresponding to the axion mass  $m_a \approx 10^{-4}$  eV) and which enters all the computations is consistent with all known astrophysical, cosmological, satellite, and ground-based constraints as highlighted above. Furthermore, in a number of cases, the predictions of the model are very close to the presently

available limits, and very modest improving of those constraints may lead to a discovery of the nuggets. Even more than that, there is a number of frequency bands where some excess of emission was observed, and this model may explain some portion, or even the entire excess, of the observed radiation in these frequency bands.

In light of this (quite optimistic) assessment of the observational constraints of this model, it is quite obvious that further and deeper studies of this model are worth pursuing. The relevant developments may include, but are not limited to, such hard problems as formation mechanisms during the QCD phase transition in the early Universe, even though many key elements for properly addressing those questions at  $\theta \neq 0, \mu \neq 0, T \neq 0$  are still largely unknown in strongly coupled QCD as shown on Fig. 1. This work is the first step in the direction toward exploring a possible mechanism of the formation of the nuggets.

### III. FORMATION OF THE NUGGETS: THE CRUCIAL INGREDIENTS OF THE PROPOSAL

1. First important element of this proposal is the presence of the topological objects, the axion domain walls [36]. As we already mentioned, the  $\theta$  parameter is the angular variable and therefore supports various types of the domain walls, including the so-called  $N_{DW} = 1$  domain walls when  $\theta$  interpolates between one and the same physical vacuum state with the same energy  $\theta \rightarrow \theta + 2\pi n$ . The axion domain walls may form at the same moment when the axion potential gets tilted, i.e., at the moment  $T_a$  when the axion field starts to roll due to the misalignment mechanism. The tilt becomes much more pronounced at the phase transition when the chiral condensate forms at  $T_c$ . In general, one should expect that the  $N_{DW} = 1$  domain walls form once the axion potential is sufficiently tilted, i.e., anywhere between  $T_a$  and  $T_c$ .

One should comment here that it is normally assumed that for the topological defects to be formed the Peccei-Quinn (PQ) phase transition must occur after inflation. This argument is absolutely correct for a generic type of domain walls with  $N_{DW} \neq 1$ . The conventional argument is based on the fact that few physically *different vacua* with the same energy must be present inside of the same horizon for the domain walls to be formed. The  $N_{DW} = 1$  domain walls are unique and very special in the sense that  $\theta$  interpolates between *one and the same* physical vacuum state. Such  $N_{DW} = 1$  domain walls can be formed even if the PQ phase transition occurred before inflation and a unique physical vacuum occupies entire Universe; see some elaboration of this point at the end of this section.

It has been realized many years after [36] that the walls, in general, demonstrate a sandwichlike substructure on the QCD-scale  $\Lambda_{\text{QCD}}^{-1} \approx \text{fm}$ . The arguments supporting the QCD-scale substructure inside the axion domain walls

are based on analysis [37] of QCD in the large- $N$  limit with the inclusion of the  $\eta'$  field<sup>4</sup> and independent analysis [39] of supersymmetric models where a similar  $\theta$  vacuum structure occurs.

One should remark here that the described structure is a classically stable configuration. In particular, the  $\eta'$  field cannot decay to  $2\gamma$  simply due to the kinematical reasons when the  $\eta'$  field is off shell and cannot be expressed as a superposition of on-shell free particles. It can only decay through the tunnelling, and therefore such  $N_{DW} = 1$  domain walls are formally metastable rather than absolutely stable configurations.

2. Second important element is that, in addition to these known QCD substructures [37–39] of the axion domain walls expressed in terms of the  $\eta'$  and gluon fields, there is another substructure with a similar QCD scale which carries the baryon charge. Precisely this novel feature of the domain walls which was not explored previously in the literature will play a key role in our proposal because exactly this new effect will be eventually responsible for the accretion of the baryon charge by the nuggets. Both the quarks and antiquarks can accrete on a given closed domain wall, making eventually the quark nuggets or antinuggets, depending on the sign of the baryon charge. The sign is chosen randomly such that an equal number of quark and antiquark nuggets are formed if the external environment is  $CP$  even, which is the case when fundamental  $\theta = 0$ . One can interpret this phenomenon as a *local spontaneous symmetry-breaking effect*, when on the scales of order the correlation length  $\xi$  the nuggets may acquire the positive or negative baryon charge with equal probability, as discussed in great detail in Sec. IV.

3. Next important ingredient of the proposal is the Kibble-Zurek mechanism, which gives a generic picture of the formation of the topological defects during a phase transition; see the original papers in Ref. [40], the review in Ref. [41], and the textbook in Ref. [42]. In our context, the Kibble-Zurek mechanism suggests that, once the axion potential is sufficiently tilted, the  $N_{DW} = 1$  domain walls form. The potential becomes much more pronounced when the chiral condensate forms at  $T_c$ . Some time after  $T_a$ , the system is dominated by a single, percolated, highly folded, and crumpled domain wall of very complicated topology. In addition, there will be a finite portion of the closed walls (bubbles) with typical size of order correlation length  $\xi(T)$ , which is defined as an average distance between folded domain walls at temperature  $T$ . It is known that the probability of finding closed walls with very large size  $R \gg \xi$  is exponentially small. Furthermore, numerical

<sup>4</sup>The  $\eta'$  field has special property that it enters the effective Lagrangian in unique combination  $[\theta - \eta'(x)]$  where the  $\theta$  parameter in the present context plays the role of the axion dynamical field  $\theta(x)$ . A similar structure is known to occur in CS phase as well. The corresponding domain walls in the CS phase have been also constructed [38].

simulations suggest [42] that approximately 87% of the total wall area belongs to the percolated large cluster, while the rest is represented by relatively small closed bubbles with sizes  $R \sim \xi$ .

The key point for our proposal is the existence of these finite closed bubbles made of the axion domain walls.<sup>5</sup> One should remark here that these closed bubbles form sometime after  $T_a$  when the original  $\theta$  parameter has not settled yet to its minimum value. It implies that the domain wall evolution starts at the time when the  $\theta$  parameter is not yet zero.<sup>6</sup> Normally, it is assumed that these closed bubbles collapse as a result of the domain wall pressure and do not play any significant role in the dynamics of the system. However, as we already mentioned in the Introduction, the collapse of these closed bubbles is halted due to the Fermi pressure acting inside of the bubbles. Therefore, they may survive and serve as the dark-matter candidates.

The percolated network of the domain walls will decay to the axion in a conventional way as discussed in Refs. [43,45,46]. Those axions (along with the axions produced by the conventional misalignment mechanism [43,44]) will contribute to the dark-matter density today. The corresponding contribution to dark-matter density is highly sensitive to the axion mass as  $\Omega_{\text{dark}} \sim m_a^{-1}$ . It may saturate the observed dark-matter density if  $m_a \approx 10^{-6}$  eV [8–15], while it may contribute very little to  $\Omega_{\text{dark}}$  if the axion mass is slightly heavier than  $m_a \approx 10^{-6}$  eV. In contrast, in our framework, an approximate relation  $\Omega_{\text{dark}} \approx \Omega_{\text{visible}}$  holds irrespectively of the axion mass  $m_a$ .

We shall not elaborate on the production and spectral properties of these axions in the present work. Instead, the focus of the present paper is the dynamics of the closed bubbles, which is normally ignored in computations of the axion production. Precisely these closed bubbles, according to this proposal, will eventually become the stable nuggets and may serve as the dark-matter candidates.

As we already mentioned, the nugget's contribution to  $\Omega_{\text{dark}}$  is not very sensitive to the axion mass but rather is determined by the formation temperature  $T_{\text{form}}$  as explained in Introduction; see also footnote 3 with a few important

<sup>5</sup>The presence of such closed bubbles in numerical simulations in the context of the axion domain wall has been mentioned in Ref. [10], where it was argued that these bubbles would oscillate and emit gravitational waves. However, we could not find any further details on the fate of these closed bubbles in the literature.

<sup>6</sup>This  $\theta$  parameter in our work is defined as the value of  $\theta$  at the moment when the domain walls form. It is not exactly the same value as the misalignment angle, which normally enters all the computations due to the conventional misalignment mechanism [43,44]. This is because the temperature when the domain walls form and the temperature  $T_a$  when the axion field starts to roll do not exactly coincide though both effects are due to the same axion tilted potential. The crucial point is that the  $\theta$  parameter, as defined above, could be numerically small, but, nevertheless, it preserves its coherence over entire Universe; see item 5 below and Sec. VII for details.

comments on this. The time evolution of these nuggets after their formation is the subject of Sec. V.

4. There existence of the CS phase in QCD represents the next crucial element of our scenario. The CS has been an active area of research for quite some time; see review papers [16,17] on the subject. The CS phase is realized when quarks are squeezed to the density which is a few times nuclear density. It has been known that this regime may be realized in nature in neutron star interiors and in the violent events associated with the collapse of massive stars or collisions of neutron stars, so it is important for astrophysics.

The force which squeezes quarks in neutron stars is gravity; the force which does an analogous job in the early Universe during the QCD phase transition is a violent collapse of a bubble of size  $R \sim \xi(T)$  formed from the axion domain wall as described in item 3 above. If the number density of quarks trapped inside of the bubble (in the bulk) is sufficiently large, the collapse stops due to the internal Fermi pressure. In this case, the system in the bulk may reach the equilibrium with the ground state being in a CS phase. As we advocate in Sec. V, this is a very plausible fate of a relatively large size bubbles of size  $R \sim \xi(T)$  made of the axion domain walls which were produced after the QCD phase transition.

5. If  $\theta$  vanishes, then an equal number of nuggets and antinuggets would form. However, the  $CP$ -violating  $\theta$  parameter (the axion field), which is defined as value of  $\theta$  at the moment of domain wall formation, generically is not zero, though it might be numerically quite small. Precisely the dynamics of the coherent axion field  $\theta(x)$  leads to preferences in the formation of one species of nuggets, as discussed in Sec. VII. This sign preference is correlated on the scales where the axion field  $\theta(x)$  is coherent, i.e., on the scale of the entire Universe at the moment of the domain wall formation. In other words, we assume that the PQ phase transition happened before inflation. One should emphasize that this assumption on the coherence of the axion field on very large scales is consistent with formation of  $N_{DW} = 1$  domain walls; see item 1 above. This coherence obviously cannot be satisfied for a generic type of the domains walls with  $N_{DW} \neq 1$  when  $N_{DW}$  *physically distinct* vacuum states with the same energy must be present in the system.

There are few arguments supporting this claim. First of all, one should remember that the axion domain wall with  $N_{DW} = 1$  corresponds to the configuration when the  $\theta$  field interpolates between  $\theta = 0$  and  $\theta = 2\pi$ . It implies that the axion field, describing the domain wall, interpolates between a topologically distinct but physically identical and unique vacuum state. We present a few strong arguments below suggesting that the topological sectors must be always present in the system everywhere in space, and inflation does not remove different topological sectors from the system. Therefore,  $N_{DW} = 1$  can be formed even if the PQ phase transition happened before inflation.

The simplest way to explain this claim is to analyze the expression for vacuum energy [47,48] in the limit of a large number of colors  $N_c \rightarrow \infty$ , though it is known that the arguments still hold for finite  $N_c$  as well.<sup>7</sup> The main point is that the vacuum energy as a function of  $\theta$  assumes the form

$$E_{\text{vac}}(\theta) \sim \min_k (\theta + 2\pi k)^2 + \mathcal{O}\left(\frac{1}{N_c}\right), \quad (8)$$

where  $\theta$  in the present context plays the role of the axion field. This formula explicitly shows that for each given  $\theta$  the vacuum state is unique. However, there are a number of different branches, classified by parameter  $k$  such that when  $\theta = \pm\pi$  the system becomes double degenerate, and one branch replaces another branch at  $\theta = \pm\pi$ . Precisely this pattern provides the required  $2\pi$  periodicity of the system. This picture of the  $\theta$  dependence is commonly accepted by the community and in fact emerges in many different gauge theories where exact computations can be carried out, including the holographic description [48].

The key point in these arguments is the presence of  $k$  different branches, which must be present in the system everywhere in space in order to provide the  $2\pi$  periodicity of the vacuum energy (8). There is only one physical vacuum in the system, which, however, is always accompanied by  $k$  different branches. Inflation cannot remove different  $k$  branches outside the horizon because they are inherent elements of the system at each point in space. The domain wall solution with  $N_{DW} = 1$  corresponds to interpolation between different topological sectors  $k = 1$  and  $k = 0$ , which are always present in the system inside the same horizon.

Another argument which leads to the same conclusion goes as follows. The  $N_{DW} = 1$  is formed as a result of the twisting of the axion field in configurational space when the axion field returns to its initial physical vacuum state after making a full circle as explained above. Topologically, it is identical to the creation of solitons in the two-dimensional Sine-Gordon model  $\sim \cos \phi$  in condensed matter physics when the  $\phi$  field interpolates between one and the same physical, but topologically distinct, states  $\phi = 0$  and  $\phi = \pm 2\pi$ . In the dual picture, the Sine-Gordon solitons can be thought of as  $\psi$  fermions; see Sec. IV for references on this duality relation. In this dual picture, the production of solitons corresponds to production of the fermi  $\psi$  fields. It is quite obvious that the production of the  $\psi$  fields is a perfectly allowed process at  $T \neq 0$  irrespectively of whether inflation happened before or after the PQ

<sup>7</sup>For finite  $N_c$  in some simple models, the computations for the vacuum energy can be exactly carried out. In many cases, formula (8) assumes the form  $E_{\text{vac}}(\theta) \sim \min_k (-N_c^2) \cos\left(\frac{\theta + 2\pi k}{N_c}\right)$ , which is obviously reduced to (8) in the large- $N_c$  limit.

symmetry breaking occurred. Formally, the mere existence of the  $\psi$  field in the system is due to  $k$  topological sectors in the theory when  $\phi$  enters the Lagrangian in combination  $(\phi + 2\pi k)$ . The inflation obviously cannot remove  $k$  sectors from the system because it would violate the fundamental properties of the theory, such as duality between  $\psi$  and  $\phi$  descriptions.

For our system, it implies that the  $N_{DW} = 1$  corresponding to the interpolation between  $k = 1$  and  $k = 0$  is an allowed configuration, irrespectively of inflation, as all  $k$  topological sectors must be present in the system in every point of space-time.

To conclude this section, as we argue below, the generic consequence of this framework (1) is not very sensitive to an absolute value of  $\theta$  at the moment of the domain wall formation; see the comment in footnote 3 on this matter. One can say that the coherent axion field  $\theta(x) \neq 0$ , being numerically small, plays the role of the  $CP$ -violating catalyst, which determines a preferred direction for *separation of the baryon charges* on the Universe scale. This role of  $CP$  violation in our proposal is quite different from the role it plays in conventional baryogenesis mechanisms.

#### IV. FORMATION OF THE NUGGETS: ACCRETION OF THE BARYON CHARGE

From now on and until Sec. VII, we focus on the dynamics of a single closed bubble produced during the domain wall formation as described in item 3, Sec. III. The correlation length  $\xi(T)$  is defined as an average distance between folded domain walls at temperature  $T$ . We assume that the initial size of the bubble  $\xi(T)$  is sufficiently large, a few times larger than the axion domain wall width  $\sim m_a^{-1}$ , such that one can locally treat the surface of the closed bubble being flat.

The main goal of this section is to demonstrate that such a bubble will generically acquire a baryon (or antibaryon) charge in very much the same way as the  $\eta'$  field was dynamically accreted as originally discussed in Ref. [37] and briefly explained in item 2, Sec. III above. In other words, we shall argue in this section that the bubbles with baryon or antibaryon charge will be copiously produced during the phase transition as they are very generic configurations of the system. In both cases, the effect emerges as a result of the nontrivial boundary conditions formulated far away from the domain wall core when the field assumes physically the same but topologically distinct vacuum states on opposite sides of the axion domain wall.

The technique we shall adopt in this section has been previously used to study the generation of the magnetic field in the domain wall background [49]. This method makes the approximation that the domain wall is flat and that translational and rotational symmetries are preserved in the plane of the wall (which we take to be the  $x$ - $y$  plane).

These approximations are marginally justified in our case because the initial curvature  $R \sim \xi(T)$  is assumed to be few times larger than the width of the wall  $\sim m_a^{-1}$ .

Once this approximation is made, we can reformulate the problem in  $1 + 1$  dimensions ( $z$  and  $t$ ) and calculate the density of the bulk properties along the domain wall. To regain the full four-dimensional bulk properties, we shall estimate the density of the particles in the  $x - y$  plane to obtain the appropriate density and degeneracy factors for the bulk density.

We proceed to demonstrate this technique by computing the accumulation of baryon charge along the wall. We take the standard form for the interaction between the pseudo-scalar fields and the fermions which respect all relevant symmetries:

$$\mathcal{L}_4 = \bar{\Psi}(i\partial - m e^{i[\theta(z) - \phi(z)]\gamma_5} - \mu\gamma_0)\Psi. \quad (9)$$

Here,  $\theta(z)$  and  $\phi(z)$  are the dimensionless axion and  $\eta'$  domain wall solution. Parameter  $m$  is the typical QCD scale of the problem, while  $\mu$  is the typical chemical potential at a specific time in the evolution of the system; see below for more precise explanations. We also simplify the problem by ignoring all flavor and color indices as well as an effective four-fermion interaction, as our main goal is to explain the basic idea with a simplified setting.

The parameter  $m$  in Eq. (9) should not be literally identified with the quark mass nor with the nucleon mass. Instead, this dimensional parameter  $m \sim \Lambda_{\text{QCD}}$  should be thought of as an effective coupling in our model when parameter  $m$  effectively describes the interaction with fermion field  $\Psi$  in all phases during the formation time, including the quark gluon plasma as well as hadronic and CS phases.<sup>8</sup> The same comment also applies to a numerical value of the chemical potential  $\mu$ : it vanishes during initial time and becomes very large when the CS phase sets in inside the nugget.

The strategy is to break Eq. (9) into two  $1 + 1$ -dimensional components by setting  $\partial_x = \partial_y = 0$  (this is the approximation that the physics in the  $z$  direction decouples from the physics in the  $x - y$  plane) and then by manipulating the system of equations that result.

<sup>8</sup>In quark gluon phase, the color singlet  $\eta'$  field does not exist. However, the singlet phase which accompanied the quark field is still present in the system. The coefficient  $m$  in this phase can be computed using the instanton liquid model. At very high temperature, the parameter  $m$  is proportional to the quark masses and is indeed very small. When temperature decreases, the instanton contribution grows very fast. At this point, parameter  $m$  is proportional to the vacuum expectation value of the 't Hooft determinant. When the temperature further decreases, the parameter  $m$  is proportional to the diquark condensate in the CS phase or the chiral condensate in the hadronic phase; see Fig. 1. We shall not elaborate along this line by assuming  $m \sim \Lambda_{\text{QCD}}$  for all our estimates which follow.

First, we introduce the following chiral components of the Dirac spinors,<sup>9</sup>

$$\Psi_+ = \frac{1}{\sqrt{S}} \begin{pmatrix} \chi_1 \\ \chi_2 \end{pmatrix}, \quad \Psi_- = \frac{1}{\sqrt{S}} \begin{pmatrix} \xi_1 \\ \xi_2 \end{pmatrix}, \quad (10)$$

$$\Psi = \frac{1}{\sqrt{2S}} \begin{pmatrix} \chi_1 + \xi_1 \\ \chi_2 + \xi_2 \\ \chi_1 - \xi_1 \\ \chi_2 - \xi_2 \end{pmatrix} = \frac{1}{\sqrt{2}} \begin{pmatrix} \Psi_+ + \Psi_- \\ \Psi_+ - \Psi_- \end{pmatrix}, \quad (11)$$

where  $S$  is the area of the wall. This normalization factor cancels the degeneracy factor proportional to  $S$  added in the text below.

The associated Dirac equation is

$$\begin{pmatrix} -me^{i(\phi-\theta)} & i(\partial_t + \partial_z) - \mu \\ i(\partial_t - \partial_z) - \mu & -me^{-i(\phi-\theta)} \end{pmatrix} \begin{pmatrix} \chi_1 \\ \xi_1 \end{pmatrix} = 0, \quad (12a)$$

$$\begin{pmatrix} -me^{i(\phi-\theta)} & i(\partial_t - \partial_z) - \mu \\ i(\partial_t + \partial_z) - \mu & -me^{-i(\phi-\theta)} \end{pmatrix} \begin{pmatrix} \chi_2 \\ \xi_2 \end{pmatrix} = 0, \quad (12b)$$

where we decouple the  $z$  coordinates from  $x$  and  $y$  by setting  $\partial_x = \partial_y = 0$ . Remember that we are looking for a two-dimensional Dirac equation, and thus we want the kinetic terms to look the same. For this reason, we should flip the rows and columns of the second equation. Doing this and defining the two two-dimensional spinors

$$\begin{aligned} \Psi_{(1)} &= \begin{pmatrix} \chi_1 \\ \xi_1 \end{pmatrix}, \\ \Psi_{(2)} &= \begin{pmatrix} \xi_2 \\ \chi_2 \end{pmatrix}, \end{aligned} \quad (13)$$

the equations have the structure

$$(i\hat{\gamma}^\nu \partial_\nu - me^{+i(\theta-\phi)\hat{\gamma}_5} - \mu\hat{\gamma}_0)\Psi_{(1)} = 0 \quad (14a)$$

$$(i\hat{\gamma}^\nu \partial_\nu - me^{-i(\theta-\phi)\hat{\gamma}_5} - \mu\hat{\gamma}_0)\Psi_{(2)} = 0 \quad (14b)$$

where the index  $\nu \in \{t, z\}$ , the Lorentz signature is  $(1, -1)$ , and we define the following two-dimensional version of the gamma matrices:

<sup>9</sup>We are using the standard representation here:

$$\begin{aligned} \gamma_0 &= \begin{pmatrix} I & 0 \\ 0 & -I \end{pmatrix}, & \gamma_j &= \begin{pmatrix} 0 & \sigma_j \\ -\sigma_j & 0 \end{pmatrix}, & \gamma_5 &= \begin{pmatrix} 0 & I \\ I & 0 \end{pmatrix}, \\ \sigma_1 &= \begin{pmatrix} 0 & 1 \\ 1 & 0 \end{pmatrix}, & \sigma_2 &= \begin{pmatrix} 0 & -i \\ i & 0 \end{pmatrix}, & \sigma_3 &= \begin{pmatrix} 1 & 0 \\ 0 & -1 \end{pmatrix}. \end{aligned}$$

$$\hat{\gamma}_t = \sigma_1, \quad \hat{\gamma}_z = -i\sigma_2, \quad \hat{\gamma}_5 = \sigma_3.$$

These satisfy the proper two-dimensional relationships  $\hat{\gamma}_5 = \hat{\gamma}_t \hat{\gamma}_z$  and  $\hat{\gamma}_\mu \hat{\gamma}_\nu = g_{\mu\nu} + \epsilon_{\mu\nu} \hat{\gamma}_5$ . We can reproduce Eq. (14) from the effective two-dimensional Lagrangian density

$$\begin{aligned} \mathcal{L}_2 &= \bar{\Psi}_{(1)} (i\hat{\gamma}^\mu \partial_\mu - me^{+i(\theta-\phi)\hat{\gamma}_5} - \mu\hat{\gamma}_0) \Psi_{(1)} \\ &+ \bar{\Psi}_{(2)} (i\hat{\gamma}^\mu \partial_\mu - me^{-i(\theta-\phi)\hat{\gamma}_5} - \mu\hat{\gamma}_0) \Psi_{(2)}, \end{aligned} \quad (15)$$

where two different species of fermion with opposite chiral charge interact with the axion domain wall background determined by the  $\theta(z)$  and  $\phi(z)$  fields. Note that, due to the normalization factor  $1/\sqrt{S}$  we introduced above, the two-dimensional fields  $\Psi_{(i)}$  have the correct canonical dimension  $1/2$ .

We have thus successfully reduced our problem to a two-dimensional fermionic system. It is known that for several systems in  $1+1$  dimensions the fermionic representation is equivalent to a  $1+1$ -dimensional bosonic system through the following equivalences [50,51]:

$$\bar{\Psi}_{(j)} i\hat{\gamma}^\mu \partial_\mu \Psi_{(j)} \rightarrow \frac{1}{2} (\partial_\mu \theta_j)^2, \quad (16a)$$

$$\bar{\Psi}_{(j)} \hat{\gamma}_\mu \Psi_{(j)} \rightarrow \frac{1}{\sqrt{\pi}} \epsilon_{\mu\nu} \partial^\nu \theta_j, \quad (16b)$$

$$\bar{\Psi}_{(j)} \Psi_{(j)} \rightarrow -m_0 \cos(2\sqrt{\pi}\theta_j), \quad (16c)$$

$$\bar{\Psi}_{(j)} i\hat{\gamma}_5 \Psi_{(j)} \rightarrow -m_0 \sin(2\sqrt{\pi}\theta_j). \quad (16d)$$

The constant  $m_0$  in the last two equations is a dimensional parameter of order  $m_0 \sim m \sim \Lambda_{\text{QCD}}$ . The exact coefficient of this factor depends on the renormalization procedure and is only known for few exactly solvable systems but in all cases is of order unity.

After making these replacements, we are left with the following two-dimensional bosonic effective Lagrangian density describing the two fields  $\theta_1$  and  $\theta_2$  in the domain wall background determined by  $\phi(z)$  and  $\theta(z)$ ,

$$\mathcal{L}_2 = \frac{1}{2} (\partial_\mu \theta_1)^2 + \frac{1}{2} (\partial_\mu \theta_2)^2 - U(\theta_1, \theta_2) + \frac{\mu}{\sqrt{\pi}} \frac{\partial(\theta_2 + \theta_1)}{\partial z}, \quad (17)$$

where the effective potential is

$$\begin{aligned} U(\theta_1, \theta_2) &= -mm_0 [\cos(2\sqrt{\pi}\theta_1 - \phi + \theta)] \\ &- mm_0 [\cos(2\sqrt{\pi}\theta_2 + \phi - \theta)]. \end{aligned} \quad (18)$$

The conventional procedure to study the system (17) is to add the kinetic terms for the axion  $\theta$  and the  $\eta'$  field  $\phi$

into (17) and study a resulting solution depending on four dynamical fields by specifying all possible boundary conditions when the potential energy (18) assumes its minimal value.<sup>10</sup> In other words, one should take into account the dynamics of the  $\theta$  and  $\phi$  fields together with  $\theta_1$ ,  $\theta_2$  because the typical scales for  $\phi$ ,  $\theta_1$ ,  $\theta_2$  are roughly the same order of magnitude and of order of  $\Lambda_{\text{QCD}}$ . To recapitulate it, one cannot study the dynamics of the  $\theta_1$ ,  $\theta_2$  field by neglecting their backreaction on the background axion and  $\phi$  fields.

For our present purposes, however, we do not really need explicit profile functions for a large number of different domain walls determined by various boundary conditions controlled by Eq. (18). The only important element relevant for our future discussions is the observation that some of the domain walls may carry the baryon (antibaryon) charge. Indeed, the domain walls which satisfy the boundary conditions

$$\begin{aligned} 2\sqrt{\pi}\theta_1(z = +\infty) - 2\sqrt{\pi}\theta_1(z = -\infty) &= 2\pi n_1 \\ 2\sqrt{\pi}\theta_2(z = +\infty) - 2\sqrt{\pi}\theta_2(z = -\infty) &= 2\pi n_2 \end{aligned} \quad (19)$$

carry the baryon charge  $N$  defined for one particle Dirac equation,

$$\begin{aligned} N &= \int d^3x \bar{\Psi} \gamma_0 \Psi = \int dz (\bar{\Psi}_1 \hat{\gamma}_0 \Psi_1 + \bar{\Psi}_2 \hat{\gamma}_0 \Psi_2) \\ &= -\frac{1}{\sqrt{\pi}} \int_{-\infty}^{+\infty} dz \frac{\partial}{\partial z} (\theta_1 + \theta_2) = -(n_1 + n_2), \end{aligned} \quad (20)$$

where we express the final formula in terms of the auxiliary two-dimensional fields  $\theta_1$  and  $\theta_2$  and corresponding boundary conditions given by Eq. (19). Factor  $S$  also cancels with our normalization for the four-dimensional  $\Psi$  field.

To complete the computations for four-dimensional baryon charge  $B$  accumulated on the domain wall, we need to multiply (20) by the degeneracy factor in the vicinity of the domain wall, which can be estimated as

$$B = N \cdot g \cdot \int \frac{d^2x_{\perp} d^2k_{\perp}}{(2\pi)^2} \frac{1}{\exp(\frac{\epsilon - \mu}{T}) + 1}, \quad (21)$$

where  $g$  is an appropriate degeneracy factor, e.g.,  $g \approx N_c N_f$  in the CS phase. We note that an additional degeneracy factor 2 due to the spin is already accounted for by parameter  $N$  defined in Eq. (20). For high chemical potential  $\mu \gg T$  corresponding to the CS phase, the baryon charge per unit area accreted in the vicinity of the domain wall can be approximated as

<sup>10</sup>In fact, it was precisely the procedure which has been adopted in Ref. [37] for a similar problem of computing of the profile functions of the axion,  $\pi$  meson and  $\eta'$  domain wall described by the  $\theta - \pi - \eta'$  fields.

$$\frac{B}{S} \approx N \cdot \frac{g\mu^2}{4\pi}. \quad (22)$$

In the opposite limit of high temperature  $\mu \ll T$  which corresponds to the quark gluon plasma phase, the corresponding magnitude can be estimated as follows:

$$\frac{B}{S} \approx N \cdot \frac{g\pi T^2}{24}. \quad (23)$$

It is instructive to compare the estimate (23) with number density  $\mathcal{N}/V$  of all degrees of freedom in the vicinity of the domain wall. Assuming that the baryon charge in the domain wall background is mainly concentrated on distances of order  $m^{-1}$  from the center of the domain wall, we arrive at the estimate for the ratio of the baryon number density bound to the wall in comparison with the total number density of all degrees of freedom responsible for the thermodynamical equilibrium in this phase,

$$r \sim \frac{(B/S) \cdot m}{\mathcal{N}/V} \sim N \left( \frac{m}{T} \right) \left( \frac{\pi^3 g}{18\zeta(3)g^*} \right), \quad (24)$$

where effective degeneracy factor  $g^*$  for quark gluon plasma is  $g^* \approx [\frac{3}{4}4N_c N_f + 2(N_c^2 - 1)]$  and  $\zeta(3) \approx 1.2$  is the Riemann zeta function. Ratio (24) shows that the accreted quark density bounded to the domain wall at high temperature represents a parametrically small contribution to all thermodynamical observables mainly because of a small parameter  $m/T \ll 1$  in this phase. The situation drastically changes as we discuss in Sec. V when the temperature slowly decreases due to the expansion of the Universe and the system enters the hadronic or CS phase, as shown on Fig. 1. At this point, the baryon charge accumulation in the domain wall background becomes the major player of the system, which eventually leads to the formation of the CS nuggets or antinuggets when quarks (antiquarks) fill the entire volume of the nuggets (antinuggets).

We conclude this section with the following important comments. First, we argued that the domain walls in general accrete the baryon (or antibaryon) charge in vicinity of the center of the domain wall. The effect in many respects is similar to fractional charge localization on domain walls, while the rest of the charge is delocalized in the rest of volume of the system as discussed in the original paper [52]. The effect is also very similar to the previously discussed phenomenon on the dynamical generation of the  $\eta'$  field in the domain wall background. The key point is that at sufficiently high temperature the  $N_{\text{DW}} = 1$  domain walls form by the usual Kibble-Zurek mechanism as explained in Sec. III. The periodic fields  $\theta$ ,  $\phi$ ,  $\theta_1$ ,  $\theta_2$  may assume physically identical but topologically distinct vacuum values (20) on opposite sides of the walls. When the system cools down, the corresponding fields

inevitably form the domain wall structure, similar to analysis in hadronic [37] and CS phases [38].

We advocate the picture that the closed bubbles will be also inevitably formed as discussed in Sec. III. The collapse of these bubbles halts as a result of Fermi pressure due to the quarks accumulated inside the nugget during the evolution of the domain wall network. Section V is devoted precisely the question on the time evolution of these closed bubbles made of the  $N_{\text{DW}} = 1$  domain wall.

The most important lesson of this section is that there is a variety of acceptable boundary conditions determined by potential (18) when the energy assumes its vacuum values. Some of the domain walls will carry zero baryon charge when the combination  $(n_1 + n_2)$  vanishes according to Eq. (20). However, generically, the domain walls will acquire the baryon or antibaryon charge. This is because the domain wall tension is mainly determined by the axion field while corrections due to the QCD substructure will lead to a small correction of order  $\sim m/f_a \ll 1$ , similar to studies of the (axion  $-\eta' - \pi$ ) domain wall [37]. Therefore, the presence of the QCD substructure with nonvanishing  $(n_1 + n_2) \neq 0$  increases the domain wall tension only slightly. In other words, accumulation of the baryon charge in the vicinity of the wall does not lead to any suppression during the formation stage. Consequently, this implies that the domain closed bubbles carrying the baryon or antibaryon charge will be copiously produced during the phase transition as they are very *generic configurations of the system*. Furthermore, the baryon charge cannot leave the system during the evolution as it is strongly bound to the wall due to the topological reasons. The corresponding binding energy per quark is order of  $\mu$  and increases with time as we discuss in the next section.

This phenomenon of the “separation of the baryon charge” can be interpreted as a local version of spontaneous symmetry breaking of the baryon charge. This symmetry breaking does not occur in the entire volume in the ground state determined by the potential (18). Instead, the symmetry breaking occurs on scale  $\xi(T)$  in the vicinity of the field configurations which describe the interpolation between physically identical but topologically distinct vacuum states (19). One should add that a similar phenomenon occurs with the accumulation of the  $\eta'$  field in the vicinity of the axion domain wall as described in Ref. [37]. However, one could not term that effect as a “local spontaneous violation” of the  $U(1)_A$  symmetry because the  $U(1)_A$  symmetry is explicitly broken by anomaly, in contrast with our present studies when the baryon charge is the exact symmetry of QCD. Nevertheless, the physics is the same in a sense that the closed bubble configurations generically acquire the axial as well as the baryon charge. This phenomenon is therefore as generic as the formation of the topological domain walls themselves. On the correlation lengths of order  $\xi$ , the three periodic fields  $\phi, \theta_1, \theta_2$  may randomly assume the corresponding vacuum

values which are physically identical but topologically distinct.

Finally, one should also mention here that the very similar effect of the “local  $CP$  violation” can be experimentally tested in heavy ion collisions in an event by event basis where the so-called induced  $\theta_{\text{ind}}$  domain with a specific sign in each given event can be formed. This leads to the “charge separation effect,” which can be experimentally observed in relativistic heavy ion collisions [53]. This charge separation effect in all respects is very similar to the phenomenon discussed in the present section. In fact, the main motivation for one of the authors (A. Z.) for studies [53] was a possibility to test the ideas advocated in this work by performing a specific analysis in the controllable “little bang” heavy ion collision experiments, in contrast with “big bang,” which happened billions of years ago. This field of research initiated in Ref. [53] became the hot topic in recent years as a result of many interesting theoretical and experimental advances; see the recent review papers [54–56] on the subject.

## V. FORMATION OF THE NUGGETS: TIME EVOLUTION

We assume that a closed  $N_{\text{DW}} = 1$  domain wall has been formed as discussed in Sec. III. Furthermore, we also assume that this domain wall is classified by a nonvanishing baryon number  $(n_1 + n_2)$  according to Eq. (20). Our goal now is to study the time evolution of the obtained configuration. As we argue below, the contraction of the bubbles halts as a result of the Fermi pressure due to baryon charge accreted during the evolution. As a result, the system comes to the equilibrium at some temperature  $T_{\text{form}}$  when the nuggets complete their formation. We want to see precisely how it happens and what the typical time scales relevant for these processes are.

We start with the following effective Lagrangian describing the time evolution of the closed spatially symmetric domain wall of radius  $R(t)$ :

$$L = \frac{4\pi\sigma R^2(t)}{2} \dot{R}^2(t) - 4\pi\sigma R^2(t) + \frac{4\pi R^3(t)}{3} [P_{\text{in}}(\mu) - P_{\text{out}}(t)] + [\text{other terms}]. \quad (25)$$

Here,  $\sigma$  is the key dimensional parameter, the domain wall tension  $\sigma \sim f_\pi m_\pi f_a \sim m_a^{-1}$  as reviewed in the Introduction; see Eq. (3). The tension  $\sigma$ , in principle, is also a time-dependent parameter because the axion mass depends on time, but for qualitative analysis of this section, we ignore this time dependence for now. We return to this question later in the text. Parameters  $P_{\text{in}}[\mu(t)]$  and  $P_{\text{out}}(t)$  represent the pressure inside and outside the bubble. The outside pressure in the quark gluon plasma (QGP) phase at high temperature can be estimated as

$$P_{\text{out}} \simeq \frac{\pi^2 g^{\text{out}}}{90} T_{\text{out}}^4, \quad T_{\text{out}} \simeq T_0 \left( \frac{t_0}{t} \right)^{1/2},$$

$$g^{\text{out}} \simeq \left( \frac{7}{8} 4N_c N_f + 2(N_c^2 - 1) \right), \quad (26)$$

where  $g^{\text{out}}$  is the degeneracy factor, while  $T_0 \simeq 100$  MeV and  $t_0 \sim 10^{-4}$  s represent the initial temperature and time determined by the cosmological expansion. We also assume that the thermodynamical equilibrium is maintained at all times between inside and outside regions such that the temperature inside the bubble approximately follows the outside temperature  $T_{\text{out}}(t) \simeq T_{\text{in}}(t)$ . Very quick equilibration indeed is known to take place even in much faster processes such as heavy ion collisions. The fast equilibration in our case can be justified because the heat transport between the phases is mostly due to the light Nambu–Goldstone (NG) bosons which can easily penetrate the domain wall with little or no interaction, in contrast with quarks and baryons discussed in the previous section. This assumption will be justified *a posteriori*; see Eq. (55) on the flux exchange rate between interior and exterior regions. Therefore, we believe our approximation  $T_{\text{out}}(t) \simeq T_{\text{in}}(t)$  is sufficiently good, at least for qualitative estimates, which is the main goal of this work.

The expression for the pressure inside the bubble  $P_{\text{in}}(t)$  depends on a number of quite nontrivial features of QCD such as the bag vacuum energy, corrections due to the gap in the CS phase, and many other phenomena, to be discussed later in the text.

The equation of motion which follows from (25) is

$$\sigma \ddot{R}(t) = -\frac{2\sigma}{R(t)} - \frac{\sigma \dot{R}^2(t)}{R(t)} + \Delta P(\mu) - 4\eta \frac{\dot{R}(t)}{R(t)}, \quad (27)$$

where  $\Delta P[\mu(t)] \equiv [P_{\text{in}}(\mu) - P_{\text{out}}(t)]$ . We also inserted an additional term [which cannot be expressed in the Lagrangian formulation (25)], the shear viscosity  $\eta$  to the right-hand side of the equation, which effectively describes the “friction” of the system when the domain wall bubble moves in an “unfriendly” environment.<sup>11</sup> On the microscopical level, this term effectively accounts for a large number of different effects which do occur during the

<sup>11</sup>We use conventional normalization factor of  $4\eta \dot{R}(t)/R(t)$  for the viscous term. This normalization factor is the same as that which appears in the Rayleigh-Plesset equation in the classical hydrodynamics when the viscous term, the surface tension term  $2\sigma/R(t)$ , and the pressure term  $\Delta P$  enter the equation in a specific combination as presented in (27). One should emphasize that our equation (27) describes the dynamics of the 2D surface characterized by the same surface tension  $\sigma$  in contrast with classical equation of the Rayleigh-Plesset equation describing a 3D spherical bubble in a liquid of infinite volume. This difference explains some distinctions between the kinetic terms proportional to factor  $\sim \sigma$  in our case (27) in contrast with the classical Rayleigh-Plesset equation.

time evolution. Such processes include but are not limited to different scattering process by quarks, gluons, or Nambu–Goldstone bosons in different phases. All these particles and quasiparticles interact among themselves and also with a moving domain wall. Furthermore, the annihilation processes which take place inside the bubble and which result in the production of a large number of strongly interacting quasiparticles also contribute to  $\eta$ .

Having discussed an expression for  $P_{\text{out}}(T)$  and viscous term  $\sim \eta$ , we now wish to discuss the structure of the internal pressure  $P_{\text{in}}(\mu)$  which enters (27). It has a number of contributions which originate from very different physics. We represent  $P_{\text{in}}(\mu)$  as a combination of three terms to be discussed one by one in order,

$$P_{\text{in}}(\mu) \simeq P_{\text{in}}^{\text{(Fermi)}}(\mu) + P_{\text{in}}^{\text{(bag const)}}(\mu) + P_{\text{in}}^{\text{(others)}}. \quad (28)$$

In this formula,  $P_{\text{in}}^{\text{(Fermi)}}$  can be represented as

$$P_{\text{in}}^{\text{(Fermi)}}(\mu) = \frac{E}{3V} = \frac{g^{\text{in}}}{6\pi^2} \int_0^\infty \frac{k^3 dk}{[\exp(\frac{\epsilon(k)-\mu}{T}) + 1]}, \quad (29)$$

where we assume that quarks are massless and the chemical potential  $\mu(t)$  implicitly depends on time as a result of the bubble’s evolution (shrinking). The degeneracy factor in this formula is

$$g^{\text{in}} \simeq 2N_c N_f, \quad (30)$$

where we keep only the quark contribution by neglecting the antiquarks. In other words, we simplify the problem by ignoring the time dependence of the degeneracy factor  $g^{\text{in}}(t)$  which effectively varies as a result of  $\mu(t)$  variation.

Now, we are in position to discuss  $P_{\text{in}}^{\text{(bag constant)}}$  from (28), which can be represented as

$$P_{\text{in}}^{\text{(bag const)}}(\mu) \simeq -E_B \cdot \theta[\mu - \mu_1] \left[ 1 - \frac{\mu_1^2}{\mu^2} \right], \quad (31)$$

where positive parameter  $E_B \sim (150 \text{ MeV})^4$  is the famous “bag constant” from the MIT bag model; see Ref. [3] for references and numerical estimates for this parameter in the given context of the nugget structure. The bag constant can be expressed in terms of the gluon and quark condensates in QCD. We shall not elaborate on this problem in the present work by referring to Ref. [3] with relevant studies in the given context.

The bag “constant”  $E_B$  describes the differences of vacuum energies (and therefore, vacuum pressure) in the interior and exterior regions of the nuggets. This difference occurs in our context because the phases realized outside and inside of the nugget are drastically distinct. For example, at the end of formation, the outside region of the nugget is in a cold hadronic phase, while the inside

region is in the CS phase. The vacuum energies in these two phases are known to be drastically different. This term works as a squeezer, similar to the role it plays in the MIT bag model, when the vacuum energy outside of the nugget is lower than the vacuum energy inside the nugget. Therefore, it enters with the same sign minus as the domain wall pressure.

A specific  $\mu$  dependence used in (31) is an attempt to model a known feature of QCD in which the absolute value of the vacuum energy decreases when the chemical potential increases. This feature is well established and tested in conventional nuclear matter physics, and it was analytically derived in a simplified version of QCD with number of colors  $N_c = 2$ ; see Ref. [3] for references and details. Our parametrization (31) corresponds to the behavior when  $P_{\text{in}}^{\text{(bag constant)}}(\mu) = 0$  for small chemical potentials  $\mu \leq \mu_1$  when the vacuum energies inside and outside of the nuggets are approximately equal. This term becomes the very important squeezer at large chemical potential at  $\mu \geq \mu_1$  when the system outside is in the hadronic vacuum state while inside it is in a CS phase. The numerical value for parameter  $\mu_1$  can be estimated as  $\mu_1 \sim 330$  MeV [3] when the baryon density is close to the nuclear matter density.

The last term entering (28) and coined as  $P_{\text{in}}^{\text{(others)}}(\mu)$  is due to a large number of other effects which we ignore in the present work. In particular, there is a conventional contribution due to the boson degrees of freedom which cancels the corresponding portion of  $g^{\text{out}}$  from (26) at high temperature,  $T \gg \mu$ . It does not play any important role in our analysis because we are mainly concerned with analysis of fermion degrees of freedom and building the chemical potential inside the bubble. Another effect which is worth mentioning is the formation of the gap in the CS phase due to the quark pairing, similar to the formation of the gap in conventional superconductors. The generation of the gap obviously decreases the energy of the system. There are many other phenomena which are known to occur in the CS phase [16]. However, we expect that these effects are less important in comparison with the dominating contributions which are explicitly written down, Eqs. (29) and (31).

Equation (27) can be numerically solved for  $R(t)$  if time variation of the chemical potential  $\mu(t)$  entering (29) and (31) is known. To study the corresponding time evolution for the chemical potential  $\mu(t)$ , we use expression (21) for the baryon charge bounded to the domain wall. We assume that the thermodynamical equilibrium is maintained between internal and external parts of the nugget such that  $T_{\text{in}}(t) \simeq T_{\text{out}}(t)$ . This assumption will be justified *a posteriori*; see the discussions after Eq. (55). At the same time, the chemical potential is quickly increasing with time inside the nugget due to the decreasing of the nugget's size. We also assume a fast equilibration for the chemical potential within the nugget in its entire volume. In other words, we describe the system using one and the same

chemical potential in the vicinity of the wall and deep inside the bubble. Justification for this assumption will be given later in the text.

With this picture in mind, we proceed by differentiating Eq. (21) with respect to time to arrive at the implicit equation relating  $\mu(t)$  and  $R(t)$  at fixed temperature  $T$ ,

$$\dot{B} = \frac{Ng}{4\pi^2} \dot{S}(t) \int \frac{d^2 k_{\perp}}{[\exp(\frac{\epsilon - \mu(t)}{T}) + 1]} + \frac{NgS}{4\pi^2} \frac{\dot{\mu}(t)}{T} \int \frac{d^2 k_{\perp} [\exp(\frac{\epsilon - \mu(t)}{T})]}{[\exp(\frac{\epsilon - \mu(t)}{T}) + 1]^2} + (\text{fluxes}) = 0, \quad (32)$$

where the term ‘‘fluxes’’ in (32) describes the loss of baryonic matter due to annihilation and other processes describing incoming and outgoing fluxes, to be discussed later in the text. The relation (32) gives an implicit relation between  $\mu(t)$  and  $R(t)$  which can be used for numerical studies of our Eq. (27) describing the time evolution of the system.

We shall discuss the physics related to incoming and outgoing fluxes in Appendix A. If we neglect this term which describes the loss of baryonic matter, we can analytically solve (32) for small  $\mu \ll T$  when one can use the Taylor expansion of the integrals entering (32). The result is

$$(\mu(t) - \mu_0) \simeq \frac{\pi^2 T}{6 \ln 2} \ln \left( \frac{R_0}{R(t)} \right), \quad (33)$$

where  $R_0$  is the initial size of the system at  $t = t_0$ , while  $\mu_0 \simeq 0$  is the initial chemical potential. One can explicitly see that the chemical potential builds in very fast when the nugget reduces its size only slightly. This formula (33) is only justified for very small  $\mu(t)$ . For larger values of  $\mu$ , one should use the exact formula (32).

Finally, one should note that at the end of formation at time  $t \rightarrow \infty$  when temperature  $T \ll \mu$  the evolution stops, in which case all derivatives vanish,  $\dot{R}_{\text{form}} = \dot{R}_{\text{form}} = \dot{\mu}_{\text{form}} = 0$ . At this point, the nugget assumes its final configuration with size  $R \simeq R_{\text{form}}$ , and Eq. (27) assumes the form

$$\frac{2\sigma}{R_{\text{form}}} = P_{\text{in}} = \frac{g^{\text{in}} \mu^4}{24\pi^2} - E_B \left( 1 - \frac{\mu_1^2}{\mu^2} \right), \quad \mu \geq \mu_1. \quad (34)$$

This condition is precisely the equilibrium condition studied in Ref. [3] with a few neglected contributions (such as the quark-quark interaction leading to the gap). This is of course the expected result as the time evolution, which is the subject of the present work, must lead to the equilibrium configuration when the free energy assumes its minimum determined by (34).

One should recall that analysis of the equilibrium presented in Ref. [3] with typical QCD parameters strongly

suggests that the system indeed falls into the CS phase when the axion domain wall pressure  $\sigma$  assumes its conventional value. At the same time, the equilibrium is not likely to emerge with the same typical QCD parameters without an additional external pressure related to the axion domain wall. In this sense, the axion domain wall with extra pressure due to  $\sigma \neq 0$  plays the role of an additional squeezer stabilizing the nuggets.

The key element of this section is Eq. (32), which is the direct consequence of a spontaneous accretion of the baryon (or antibaryon) charge in the domain wall background as discussed in Sec. IV. Precisely this equation explicitly shows that the chemical potential  $\mu(t)$  grows very fast when the domain wall shrinks as a result of the domain wall pressure  $\sigma$ . The presence of a nonvanishing chemical potential in the vicinity of the domain wall obviously implies the generation of the binding forces between the fermions and the domain wall, such that a typical bound energy of a single fermion to the domain wall is of order of  $\mu$ .

A generic solution of Eqs. (27) and (32), as we discuss in the next section, shows an oscillatory behavior of  $R(t)$  with a slow damping of the amplitude such that the system eventually settles down at the equilibrium point (34). However, even the very first oscillation with initial  $\mu_0 \approx 0$  leads to very fast growth of the chemical potential  $\mu(t) \approx T$  as analytical estimates represented by Eq. (33) show. In next section, we develop a quantitative framework which allows us to analyze our basic equation (27) for  $R(t)$  where time dependence  $\mu(t)$  is implicitly expressed in terms of the same variable  $R(t)$  as determined by (32).

## VI. FORMATION OF THE NUGGETS: QUALITATIVE ANALYSIS

Our goal in this section is to solve for  $R(t)$  and therefore  $\mu(t)$  by solving (27) and (32), which implicitly relate both variables. We shall observe that a nugget experiences a large number of oscillations during its evolution with slow damping rate and eventually settles down at the equilibrium point (34). This behavior of the system will be coined as “underdamped oscillations.” In Sec. VI A, we formulate some assumptions and present the technical details, while the interpretation of the obtained results will be presented in Sec. VI B. We want to make a number of simplifications in our analysis in the present section to demonstrate the generic features of these oscillations. The numerical studies presented in Appendixes A, B, and C support our basic picture of oscillatory behavior advocated in this section.

### A. Assumptions, approximations, and simplifications

Exact analytical analysis of either (27) or (32) can be obtained only during the first moment of the initial stage of the evolution of the system when  $\mu$  is sufficiently small (33). We need to understand the behavior of the system for

a much longer period of time. Thus, we make two important technical simplifications to proceed with our qualitative analysis. The first one is to neglect the term in (32) describing the fluxes. This assumption will be supported by some estimates presented in Appendix A, which show that incoming and outgoing fluxes cancel each other with very high accuracy, such that net flux is indeed quite small. Hence, Eq. (32) is now simplified to

$$\dot{B} = \frac{d}{dt} \left\{ \frac{Ng}{4\pi^2} S \int \frac{d^2 k_{\perp}}{\exp(\frac{\epsilon - \mu}{T}) + 1} \right\} = 0, \quad (35)$$

which means in this approximation that the baryonic charge is roughly conserved in the domain wall background at all times during the evolution of the system.

As our second simplification, we neglect the mass of the fermions in comparison with temperature  $T$  and the chemical potential  $\mu$ ; i.e., we use the dispersion relation  $\epsilon = \sqrt{k_{\perp}^2 + m^2} \approx k_{\perp}$  in the vicinity of the domain wall. This approximation is somewhat justified in the QGP and CS phases and is therefore along path 3 as shown on Fig. 1. It is not literally justified for paths 1 and 2 as in the hadronic phase where the quark mass  $m$  should be identified with the so-called constituent quark mass which is proportional to the chiral condensate. Nevertheless, to simplify the problem, we neglect the mass  $m(T)$  for all paths in our qualitative analysis of the time evolution as we do not expect any drastic changes in our final outcome as a result of this technical simplification. With these assumptions, we can approximate the integral entering Eq. (35) as

$$\begin{aligned} \int_0^{\infty} \frac{dk_{\perp} \cdot k_{\perp}}{e^{\frac{\epsilon(k_{\perp}) - \mu}{T}} + 1} &= T^2 \cdot I\left(\frac{\mu}{T}\right) \\ I\left(\frac{\mu}{T}\right) &\approx \frac{\pi^2}{6} + \frac{1}{2} \left(\frac{\mu}{T}\right)^2 - \frac{\pi^2}{12} e^{-\mu/T} \\ &\quad + \mathcal{O}\left(\frac{\mu}{T} e^{-\mu/T}\right), \end{aligned} \quad (36)$$

where the omitted terms  $\sim \frac{\mu}{T} e^{-\mu/T}$  will be neglected thereafter, as they will never dominate in either the small nor large limit of  $\mu$ . One can numerically check that approximation (36) describes the relevant integral  $I(\frac{\mu}{T})$  sufficiently well in the entire parametrical space of  $\mu/T$ ; see Appendix C for a corresponding analysis. As a quick test of this approximation, one can check that the approximate expression (36) reproduces an exact (in the small- $\mu$  limit) expression (33) with an accuracy of order 15%, which is more than sufficient for our qualitative studies of this section.

As mentioned above, if flux term (32) is neglected, the curly bracket term in (35) is a conserved quantity. Equating it to its initial values where  $S(t=0) = 4\pi R_0^2$ ,  $\mu(t=0) = \mu_0 \approx 0$ , one arrives at

$$T^2 R^2 \left[ \frac{\pi^2}{6} + \frac{1}{2} \left( \frac{\mu}{T} \right)^2 - \frac{\pi^2}{12} e^{-\mu/T} \right] = \frac{\pi^2}{12} T_0^2 R_0^2. \quad (37)$$

In what follows, we assume that the thermodynamical equilibration is established very quickly such that one can approximate  $T \simeq T_0$  during the time evolution as we already discussed in Sec. V. To simplify the system further, we wish to represent the equation relating  $R$  and  $\mu/T$  in the form

$$f(R) \equiv \frac{\pi^2}{6} \left[ \frac{1}{2} \left( \frac{R_0}{R} \right)^2 - 1 \right] = \frac{1}{2} \left( \frac{\mu}{T} \right)^2 - \frac{\pi^2}{12} e^{-\mu/T}, \quad (38)$$

where we introduced function  $f(R)$  for convenience of the analysis which follows. Essentially, the idea here is to simplify the basic equation (27) as much as possible to express the  $\mu(t)$ -dependent terms entering through the pressure (28) in terms of  $R(t)$  such that Eq. (27) would assume a conventional differential equation form for a single variable  $R(t)$ .

Our next step is to simplify the expression for the Fermi pressure (29) entering (28) using the same procedure we used to approximate formula (36), i.e.,

$$\begin{aligned} P_{\text{in}}^{(\text{Fermi})} &= \frac{g^{\text{in}}}{6\pi^2} \int_0^\infty \frac{k^3 dk}{\exp(\frac{\epsilon(k)-\mu}{T}) + 1} \\ &\simeq \frac{g^{\text{in}} T^4}{6\pi^2} \left\{ \frac{7\pi^4}{60} + \frac{\pi^2}{2} \left( \frac{\mu}{T} \right)^2 - \frac{7\pi^4}{120} e^{-\mu/T} \right. \\ &\quad \left. + \frac{1}{4} \left( \frac{\mu}{T} \right)^4 + \mathcal{O}\left( \frac{\mu}{T} e^{-\mu/T} \right) \right\} \\ &\simeq \frac{g^{\text{in}} T^4}{6} \left\{ \frac{7\pi^2}{60} + \left[ \frac{1}{2} \left( \frac{\mu}{T} \right)^2 - \frac{\pi^2}{12} e^{-\mu/T} \right] + \frac{1}{4\pi^2} \left( \frac{\mu}{T} \right)^4 \right\} \\ &\quad + \frac{g^{\text{in}} T^4}{6} \left\{ \frac{\pi^2}{40} e^{-\mu/T} + \mathcal{O}\left( \frac{\mu}{T} e^{-\mu/T} \right) \right\}. \quad (39) \end{aligned}$$

In what follows, we neglect the last line in Eq. (39). The justification for this procedure is the same as before: it produces a small contribution in entire region of  $\mu$  in comparison with accounted terms. The technical advantage for this procedure is the possibility to rewrite (39) in terms of the function of  $R(t)$ , rather than  $\mu(t)$  using our relation (38).

The formula in the square bracket in (39) is just  $f(R)$  defined by (38). The remaining  $(\frac{\mu}{T})^4$  term can be also expressed in terms of  $R$  by taking the square of (38),

$$\begin{aligned} f^2(R) &= \left[ \frac{1}{2} \left( \frac{\mu}{T} \right)^2 - \frac{\pi^2}{12} e^{-\mu/T} \right]^2 \\ &\simeq \frac{1}{4} \left( \frac{\mu}{T} \right)^4 + \left( \frac{\pi^2}{12} \right)^2 + \mathcal{O}\left( \frac{\mu}{T} e^{-\mu/T} \right), \quad (40) \end{aligned}$$

where the correction term  $\sim \mathcal{O}(\mu e^{-\mu/T})$  will be dropped in what follows, as before. Furthermore, we approximated a

numerically small term as follows:  $(\frac{\pi^2}{12} e^{-\mu/T})^2 \sim (\frac{\pi^2}{12})^2$ . This approximation is obviously justified for small  $\mu$ , while for large  $\mu$ , this correction is negligible anyway in comparison with the leading terms in the expression for  $P_{\text{in}}^{(\text{Fermi})}$ ; see the expression below. With these simplifications in mind, we approximate  $P_{\text{in}}^{(\text{Fermi})}$  in terms of  $R(t)$  as follows:

$$P_{\text{in}}^{(\text{Fermi})} \simeq \frac{g^{\text{in}} T^4}{6} \left[ \frac{7\pi^2}{60} + f(R) + \frac{f^2(R)}{\pi^2} - \frac{\pi^2}{144} \right]. \quad (41)$$

The expression for the Fermi pressure  $P_{\text{in}}^{(\text{Fermi})}(R)$  is now expressed in terms of  $R$  rather than in terms of  $\mu$  as in the original expression (29).

We wish to simplify the expression for  $P_{\text{in}}^{(\text{bag const})}(\mu)$  entering (28) in a similar manner to express  $P_{\text{in}}^{(\text{bag const})}$  in terms of  $R$ . This contribution becomes important as discussed after Eq. (31) only for sufficiently large  $\mu$ . In this region,  $f(R)$  can be well approximated as

$$f(R) \simeq \frac{1}{2} \left( \frac{\mu}{T} \right)^2, \quad \mu \gg T \quad (42)$$

so that we have

$$P_{\text{in}}^{\text{bag}} \simeq -E_B \cdot \theta \left( \sqrt{2f(R)} - \frac{\mu_1}{T} \right) \left( 1 - \frac{\mu_1^2}{2T^2 f(R)} \right). \quad (43)$$

As a result of these simplifications and approximations, the pressure term which enters the basic equation (27),  $\Delta P(\mu) \equiv [P_{\text{in}}(\mu) - P_{\text{out}}(t)]$ , which was initially formulated in terms of the chemical potential  $\mu$  inside the bubble, can be now written entirely in terms of a single variable, the size of the bubble  $R(t)$ ,

$$\begin{aligned} \Delta P[f(R)] &\simeq \frac{g^{\text{in}} \pi^2}{6} T^4 \left[ \frac{79}{720} - \frac{g^{\text{out}}}{15g^{\text{in}}} + \frac{f(R)}{\pi^2} + \frac{f^2(R)}{\pi^4} \right] \\ &\quad - E_B \cdot \theta \left( \sqrt{2f(R)} - \frac{\mu_1}{T} \right) \left( 1 - \frac{\mu_1^2}{2T^2 f(R)} \right), \quad (44) \end{aligned}$$

where  $f(R)$  is defined by Eq. (38). With these technical simplifications, the basic equation (27) can now be written as a second-order differential equation entirely in terms of  $R(t)$  rather than  $\mu$ ,

$$\sigma \ddot{R}(t) = -\frac{2\sigma}{R} - \frac{\sigma \dot{R}^2}{R} + \Delta P[f(R)] - 4\eta \frac{\dot{R}}{R}, \quad (45)$$

with  $\Delta P[f(R)]$  determined by Eq. (44).

This equation can be solved numerically. In fact, it is precisely the subject of Appendix B. However, the most important quantitative features of the obtained solution can be understood without any numerical studies but rather

using a simplified analytical analysis, which is precisely the subject of the next section.

### B. Time evolution: Qualitative analysis

As we already mentioned, a nugget assumes its final form at  $t \rightarrow \infty$  when all time derivatives vanish and the equation for the equilibrium is given by (34) at  $T = 0$ . In this section, we generalize this equation for the equilibrium by defining  $R_{\text{form}}(T)$  as the solution of Eq. (46), see below, at  $T \neq 0$ . In other words, the starting point of the present analysis at  $T \neq 0$  is the equilibrium condition when the ‘‘potential’’ energy assumes its minimal value. The corresponding minimum condition is determined by the equation

$$\frac{2\sigma}{R_{\text{form}}} = \Delta P(R_{\text{form}}), \quad (46)$$

where  $\Delta P(R_{\text{form}})$  is defined by Eq. (44). This condition obviously reduces to Eq. (34) at  $t \rightarrow \infty$  when  $\mu \gg T$ .

We follow the conventional technique and expand (45) around the equilibrium value  $R_{\text{form}}(T)$  to arrive to an equation for a simple damping oscillator,

$$\frac{d^2(\delta R)}{dt^2} + \frac{2}{\tau} \frac{d(\delta R)}{dt} + \omega^2(\delta R) = 0, \quad (47)$$

where  $\delta R \equiv [R(t) - R_{\text{form}}]$  describes the deviation from the equilibrium position, while new parameters  $\tau$  and  $\omega$  describe the effective damping coefficient and frequency of the oscillations. Both new coefficients are expressed in terms of the original parameters entering (45) and are given by

$$\tau = \frac{\sigma}{2\eta} R_{\text{form}} \quad (48a)$$

$$\omega^2 = -\frac{1}{\sigma} \left. \frac{d\Delta P(R)}{dR} \right|_{R_{\text{form}}} - \frac{2}{R_{\text{form}}^2}. \quad (48b)$$

The expansion (47) is justified, of course, only for small oscillations about the minimum determined by Eq. (46), while the oscillations determined by the original equation (45) are obviously not small. However, our simple analytical treatment (47) is quite instructive and gives a good qualitative understanding of the system. Our numerical studies presented in Appendix B fully support the qualitative picture presented below.

We start our qualitative analysis with estimates of the parameter  $\omega$  which depends on  $\frac{d\Delta P(R)}{dR}$  computed at  $R = R_{\text{form}}$  according to (48b). First of all, in this qualitative analysis, we neglect the bag constant term  $P_{\text{in}}^{(\text{bag constant})}$  because it only starts to play a role for sufficiently large  $\mu \geq \mu_1 \sim 330$  MeV, when formation is almost completed. This term obviously cannot change the qualitative behavior of the system discussed below. Our numerical studies

presented in Appendix B (where the bag constant term  $\sim E_B$  is included in the analysis) support this claim.

The key element for our simplified analysis is the observation that the ratio  $(R_0/R_{\text{form}})^2 \geq 14$  is expected to be a numerically large number. This expectation will be soon confirmed *a posteriori*. This observation considerably simplifies our qualitative analysis because in this case  $\Delta P(R_{\text{form}})$  defined by (44) can be approximated by a single term  $\sim f^2(R)$  in square brackets in (44) as this term essentially saturates  $\Delta P(R_{\text{form}})$ . This is because the function  $f(R)/\pi^2$  becomes numerically large in the relevant region  $f(R)/\pi^2 \sim (R_0/R_{\text{form}})^2$  according to (38).

With these simplifications, we can now estimate  $\omega^2$  as follows:

$$\omega^2 \approx \left( \frac{g^{\text{in}} \pi^2}{216} \right) \cdot \left( \frac{T^4}{\sigma R_{\text{form}}} \right) \cdot \left( \frac{R_0}{R_{\text{form}}} \right)^4 - \left( \frac{2}{R_{\text{form}}^2} \right). \quad (49)$$

To simplify the analysis further, one can represent the last term as

$$\left( \frac{2}{R_{\text{form}}^2} \right) = \left( \frac{1}{R_{\text{form}}} \right) \cdot \left( \frac{\Delta P(R_{\text{form}})}{\sigma} \right) \quad (50)$$

and keep the leading term  $\sim f^2(R)$  in the expression for  $\Delta P(R_{\text{form}})$ . One can easily convince oneself that  $\omega^2 > 0$  is always positive in this approximation such that the condition for the desired underdamped oscillations assumes a simple form,

$$\frac{f(R_{\text{form}})}{\pi^2} \gtrsim 1 \Rightarrow \left( \frac{R_0}{R_{\text{form}}} \right) \gtrsim \sqrt{14}, \quad (51)$$

when  $\Delta P(R_{\text{form}})$  defined by (44) is dominated by a single term  $\sim (\frac{f}{\pi^2})^2$ , which itself can be approximated by the leading quadratic term  $\sim (\frac{R_0}{R})^2$  according to (38). Our numerical studies presented in Appendix B support the numerical estimate (51).

One can also check that if condition (51) is not satisfied then the system shows an ‘‘overdamped’’ behavior when very few oscillations occur before the complete collapse of the system, in which case the nuggets obviously do not form. These short-lived bubbles will never get to a stage when the temperature drops below the critical value  $T_{\text{CS}}$ . Therefore, a CS phase cannot form in these ‘‘short-lived’’ bubbles. It should be contrasted with ‘‘long-lived’’ bubbles with much longer formation time of order  $\tau$ ; see the comments below.

The condition (51) is extremely important for our analysis. It essentially states that the initial size of a closed bubble  $R_0$  must be sufficiently large for a successful formation of a nugget of size  $R_{\text{form}}$ . On other hand, a formation of very large closed bubbles is strongly suppressed  $\sim \exp[-(R_0/\xi)^2]$  by the Kibble-Zurek (KZ) mechanism as reviewed in Sec. III.

This constraint will be important in our estimation of a suppression factor in Sec. VII C due to the necessity to form a sufficiently large bubble (51) during the initial stage of formation.

Assuming that condition (51) is satisfied, we estimate a typical frequency oscillations as

$$\omega \sim \frac{1}{R_{\text{form}}} \sim m_a, \quad t_{\text{osc}} \simeq \omega^{-1} \simeq m_a^{-1}, \quad (52)$$

where we used the scaling properties (3) to relate the nugget's size  $R_{\text{form}}$  with the axion mass  $m_a$ . One should emphasize that the estimate (52) is not sensitive to any approximations and simplifications we have made in our qualitative treatment of the time evolution in this section. In fact, all parameters entering relation (52) are expressible in terms of the QCD-scale  $\Lambda_{\text{QCD}}$  and a single ‘‘external’’ parameter, the axion mass  $m_a$ , which we keep unspecified at this point. Of course, we always assume that the axion mass may take any value from the observationally allowed window  $10^{-6} \text{ eV} \lesssim m_a \lesssim 10^{-3} \text{ eV}$ .

We now turn our attention to the damping coefficient defined in terms of the original parameters by Eq. (48a). It is convenient to estimate the dimensionless combination  $\omega\tau$  as

$$\omega\tau \simeq \frac{1}{R_{\text{form}}} \cdot \left( \frac{\sigma}{2\eta} R_{\text{form}} \right) \simeq \frac{\sigma}{2\eta} \sim \frac{m_\pi}{m_a} \sim 10^{11}, \quad (53)$$

where we substituted  $\omega \sim R_{\text{form}}^{-1}$  according to (52) and assumed that  $\eta \sim m_\pi^2$  has conventional QCD scale of order  $\text{fm}^{-3}$  while the wall tension  $\sigma$  can be approximated with high accuracy as  $\sigma \simeq m_\pi^4/m_a$ . This relation implies that the damping is extremely slow on the QCD scales. Therefore, the solution describing the time evolution of a long-lived bubble can be well approximated as

$$R(t) = R_{\text{form}} + (R_0 - R_{\text{form}})e^{-t/\tau} \cos \omega t, \quad (54)$$

which is obviously a solution of the approximate equation (47). This solution represents an under-damped oscillating  $R(t)$  with frequency  $\omega \sim \frac{1}{R_{\text{form}}}$  and damping time  $\tau \sim \frac{\sigma}{2\eta} R_{\text{form}}$ . Precisely these long-lived bubbles will eventually form the DM nuggets.

The time scale (53) is very suggestive and implies that the damping term starts to play a role on very large scales when the cosmological expansion of the Universe with the typical scale  $t_0 \simeq 10^{-4} \text{ s}$  must be taken into account. We have not included the corresponding temperature variation in our studies because on the QCD scales (which is the subject of the present studies) the corresponding variations are negligible. However, the estimate (53) shows that for a proper analysis of the time scales  $\tau$  the expansion of the Universe (and related to the expansion the temperature variation) must be included. The corresponding studies are

beyond the scope of the present work. However, the important comment we would like to make here is that the emergent large time scale (53) is fully consistent with our anticipation that the temperature of the Universe drops approximately by a factor of  $\sim 3$  or so when a CS phase forms in the interior of the nugget during the formation period. It is quite obvious that if the time scale (53) were considerably shorter than the cosmological time scale  $t_0 \simeq 10^{-4} \text{ s}$  then the temperature  $T \sim t^{-1/2}$  inside the nugget could not drop sufficiently deep into the region where the CS sets in as plotted on Fig. 1. Fortunately, the time scale (53) is long enough and automatically satisfies this requirement.

Now, we want to elaborate on one more element of the dynamics which is also important for a successful formation of the nuggets. To be more specific, we want to discuss the flux of particle exchange, which was ignored in our qualitative analysis in this section and which is estimated in Appendix A. This flux describes the rate of the number of particles flowing between inside and outside the system, which can be appreciably large even if the net baryonic flux is negligibly small. To be more precise, there are two kinds of fluxes, both investigated in Appendix A, that we are discussing in this paper: the net flux of baryonic charge  $\Delta\Phi \equiv \Phi_{\rightarrow} - \Phi_{\leftarrow}$  and the average flux of the particle number  $\langle\Phi\rangle \equiv \frac{1}{2}(\Phi_{\rightarrow} + \Phi_{\leftarrow})$ . The first one corresponds to the flux term entering Eq. (32), while the latter is important in understanding what is the typical time scale for a complete ‘‘refill’’ of the particles during the time evolution. The last question is important for understanding the time scale for thermal equilibration.

We start our analysis with discussions of an average flux  $\langle\Phi\rangle$  at small chemical potential. It is estimated to be  $\langle\Phi\rangle \simeq 1 \text{ fm}^{-3}$  according to Appendix A. The magnitude of this flux can be fully appreciated by computing the total number of particle exchange per one cycle of the oscillation,

$$\frac{2\pi}{\omega} \cdot 4\pi R_{\text{form}}^2 \cdot \langle\Phi\rangle \sim R_{\text{form}}^3 \text{ fm}^{-3} \sim |B|, \quad (55)$$

where  $\omega$  is a typical frequency oscillation estimated in (52) while  $|B|$  is the total number of particles (quarks and antiquarks) stored in the nugget. The physical meaning of this estimate is that a nugget can in principle entirely refill its interior with ‘‘fresh’’ particles within a few cycles of exchange. A similar estimate for the net baryon flux which includes  $\Delta\Phi$  is suppressed; see Appendix A.

The main reason for emergence of this large scale in expression (55) is a long time scale of a single cycle (52) which is determined by the axion mass  $m_a$  rather than by QCD physics. Nevertheless, estimate (55) is quite remarkable and shows that even for a very low rate of chemical potential accretion of (anti)quarks being tracked per oscillation, the high exchange rate (55) is still sufficient enough to turn a baryonically neutral nugget into one completely

filled with (anti)quarks. When the quarks become effectively massive as happens in hadronic and CS phases, the flux for the exchange of the baryon charge is drastically decreased by a factor  $\sim \exp(-m/T)$ .

The same estimate (55) essentially holds for the exchange of almost massless Nambu-Goldstone bosons for sufficiently high temperature. In fact, the lightest degrees of freedom play a crucial role in the cooling processes of the interior of the nugget as these particles can easily penetrate the sharp domain wall structure. Therefore, the high exchange rate between the exterior and interior of a nugget essentially implies that the thermal equilibrium is maintained in our system with very high precision due to a huge rate per cycle (55) when a large number of degrees of freedom  $\sim B$  have a chance of order 1 to interact with fresh particles from the exterior during a single cycle. Therefore, our assumption on the thermal equilibrium between the interior and exterior is justified *a posteriori*.

We conclude this section with few important comments. The most important result of this section is that the nuggets can be formed during the QCD phase transition, provided the initial size of the nuggets is sufficiently large as stated in Eq. (51), in which case they survive the evolution. The key role in this successful formation plays, of course, the effect of local spontaneous violation of the baryon symmetry as discussed in Sec. IV and explicitly expressed by Eqs. (19) and (20). One should emphasize that our qualitative analyses in this section are fully supported by numerical studies presented in Appendixes A and B. Therefore, we do not expect that any numerical simplifications in our analysis may drastically change the basic qualitative results presented in this section.

Another important point is the observation (52) that a typical time scale for the oscillations is of order  $t_{\text{osc}} \approx \omega^{-1} \approx m_a^{-1}$ . Both these estimates will be crucial elements in our analysis presented in Sec. VII: Eq. (51) will be important in the estimate for the efficiency of a bubble formation with a large size  $\sim R_0$ , while Eq. (52) will play a key role in our arguments, suggesting a coherent preferential formation of one type of nuggets (baryonic or antibaryonic) on the largest possible scale of the visible Universe.

## VII. BARYON CHARGE SEPARATION: CORRELATION ON COSMOLOGICAL SCALES

Until this section, we mostly concentrated on the time evolution of a single nugget (or antinugget). The main lesson of our previous discussions is that such nuggets can be formed, remain stable configurations, and therefore can serve as the dark-matter candidates. In other words, the focus of our previous studies was a problem of a local separation of charges on small scales of order the nugget's size. The key element of that separation of charges is

Eq. (19), which can be thought of as a local version of the spontaneous symmetry breaking of the baryon charge as explained in Sec. IV. However, on a larger scale, it is quite obvious that an equal number of nuggets and antinuggets will be formed as a result of an exact symmetry as we discuss below.

This symmetry, however, does not hold anymore on large scales if the axion  $CP$ -odd coupling is included in the consideration, which eventually leads to a very generic, essentially insensitive to most parameters, consequence of this framework represented by Eq. (1), which is the subject of Secs. VII A and VII B. Section VII C is devoted to some more specific and model-dependent consequences of this framework. In particular, we want to estimate a suppression factor related to a necessity to form a large size bubble (51) in the KZ mechanism.

### A. Coherent axion field as the source of $CP$ violation

First of all, let us show that the baryon charge hidden in nuggets on average is equal to the baryon charge hidden in antinuggets, of course with the sign minus. Indeed, the analysis of the antinuggets can be achieved by flipping the sign of the chemical potential in Eq. (17), i.e.,  $\mu \rightarrow -\mu$ . One can restore the original form of the  $\mu$  term in Lagrangian (17) by replacing  $\theta_1 \rightarrow -\theta_1$  and  $\theta_2 \rightarrow -\theta_2$ . Finally, one should change the signs for the axion  $\theta$  and the pseudo-scalar singlet  $\eta'$  meson represented by the  $\phi$  field in the interaction term (18) to restore the original form of the Lagrangian. These symmetry arguments imply that as long as the pseudoscalar axion field fluctuates around zero as conventional pseudoscalar fields (as  $\pi$ ,  $\eta'$  mesons, for example) the theory remains invariant under  $P$  and  $CP$  symmetries. Without this symmetry, the number density and size distribution of the nuggets and antinuggets could be drastically different.<sup>12</sup>

Therefore, the symmetry arguments suggest that on average an equal number of nuggets and antinuggets would form if the axion field is represented by a conventional quantum fluctuating field oscillating around the zero point. If it were the case, the baryons and antibaryons would continue to annihilate each other as well as annihilate with the nuggets and antinuggets in our framework. Eventually, it would lead to the Universe with large amount of dark matter in the form of nuggets and antinuggets (they are far away from each other, and therefore they do not annihilate each other) and no visible matter. However, the axion dynamics which is determined by the axion field correlated on the scale of the entire Universe leads to a preferential

<sup>12</sup>If  $\pi$  meson condensation were to occur in nuclear matter, it would unambiguously imply that the  $CP$  invariance is broken in such a phase. Some of the phases in the CS systems indeed break the  $CP$  invariance as a result of condensation of pseudoscalar Nambu-Goldstone bosons.

formation of a specific type of nuggets on the same large scales where the axion field is correlated as we argue below. Such a coherent axion field emerges if the PQ phase transition occurs before or during inflation as discussed in items 1 and 5, Sec. III.

First of all, we want to argue that the time-dependent axion field implies that there is an additional coupling to fermions (56). Indeed, by making the time-dependent  $U(1)_A$  chiral transformation in the path integral, one can always represent the conventional  $\theta$  term in the following form:

$$\Delta\mathcal{L}_4 = \mu_5(t)\bar{\Psi}\gamma_0\gamma_5\Psi \quad \mu_5 \equiv \dot{\theta}. \quad (56)$$

In this formula,  $\mu_5 \equiv \dot{\theta}$  can be thought of as the chiral chemical potential. Many interesting properties emerge in the systems if  $\mu_5$  is generated. In fact, it has been an active area of research in recent years, mostly due to very interesting experimental data suggesting that the  $\mu_5$  term can be generated in heavy ion collisions; see the original paper [53] and recent reviews [54–56] for details. In the present context, the  $\mu_5$  term is generated as a result of the axion dynamics. As a matter of fact, the original studies [53] were motivated by the proposal that the separation of the baryon charges which may occur in early Universe, as advocated in this paper, could be tested in laboratory experiments with heavy ion collisions.

Now, we are prepared to formulate the main claim of this section which can be stated as follows. When interaction (18), (56) is introduced into the system, there will be a *preferential evolution* in the system of the nuggets vs antinuggets, provided that nuggets and antinuggets had been already formed and the chemical potential  $\mu$  had been already generated locally inside the nuggets as described in Sec. VI. As we already explained earlier, the generation of  $\mu$  can be interpreted as a local violation of  $\mathcal{C}$  invariance in the system.

This preferential evolution is correlated with the  $CP$ -odd parameter on the scales where the axion field  $\theta(x)$  is coherent. In our arguments presented below, we make a standard assumption that the initial value of  $\theta(x)$  and its time derivative  $\dot{\theta}(x)$  are correlated on the entire observable Universe, such that  $\mu_5 \equiv \dot{\theta}$  is also correlated on the same large scale. Such a large-scale correlation is guaranteed if the PQ phase transition occurs before inflation; see items 1 and 5, Sec. III for details. This is the standard assumption in most studies on axion physics when one computes the present density of axions due to the misalignment mechanism; see Refs. [8–15].

For our present studies, the key element is that the dynamics of the axion field until the QCD phase transition is determined by the coherent state of axions at rest such that [8–15]

$$\theta(t) \sim \frac{C}{f^{3/4}} \cos \int^t dt' \omega_a(t'), \quad \omega_a^2(t) = m_a^2(t) + \frac{3}{16t^2}, \quad (57)$$

where  $C$  is a constant and  $t = \frac{1}{2H}$  is the cosmic time. This formula suggests that for  $m_a(t)t \gg 1$  when the axion potential is sufficiently strongly tilted the chiral chemical potential is essentially determined by the axion mass at time  $t$ :

$$\mu_5(t) = \dot{\theta}(t) \sim \omega_a(t) \simeq m_a(t). \quad (58)$$

The crucial point is that  $\theta(t)$  is one and the same in the entire Universe as it is correlated on the Universe size scale. Another important remark is that the axion field  $\theta(t)$  continues to oscillate with frequency (58) until the QCD phase transition at  $T_c$ , though its absolute value  $|\theta/\theta_0| \sim 0.01$  might be few orders of magnitude lower at  $T_c \simeq 170$  MeV than its original value  $\theta_0$  at  $T \simeq 1$  GeV when the axion field only started to roll; see, e.g., Ref. [43]. As we discuss below, the relevant physics is not very sensitive to an absolute value of  $|\theta(t)|$  in this regime, and therefore we do not elaborate further on this rather technical and computational element of the axion dynamics; see footnote 13 below for comments on this matter.

In the context of the nugget's evolution (accretion of the baryon charge), this claim implies that on the entire Universe size scale with one and the same sign of  $\theta(t)$  a specific single type of nuggets will prevail in terms of the number density and sizes. Indeed, one can present the same arguments (see the beginning of this section) with flipping the sign  $\mu \rightarrow -\mu$  with the only difference being that the interaction (18) prevents us from making the variable change  $\theta_{(i)} \leftrightarrow -\theta_{(i)}$  for a given  $\theta(t)$  because it changes its form under  $\theta_{(i)} \leftrightarrow -\theta_{(i)}$ . In other words, slow varying (on the QCD scale)  $CP$ -violating terms (18), (56) leads to a preferential evolution of the system for a specific species of the nuggets with a given sign of  $\mu$ .

Indeed, it has been known for quite some time, see, e.g., Refs. [57,58], that in the presence of  $\theta \neq 0$  a large number of different  $CP$ -violating effects take place. In particular, the Nambu-Goldstone bosons become a mixture of pseudoscalar and scalar fields, and their masses are drastically different from  $\theta = 0$  values. Furthermore, the quark chiral  $\langle \bar{\psi}\psi \rangle$  and the gluon  $\langle G^2 \rangle$  condensates become the superposition with their pseudoscalar counterparts  $\langle \bar{\psi}\gamma_5\psi \rangle$  and  $\langle G\tilde{G} \rangle$  such that entire hadron spectrum and their interactions are modified in the presence of  $\theta \neq 0$ . All these strong effects, of course, are proportional to  $\theta$  and therefore numerically suppressed in the case under consideration (57) by a factor  $|\theta/\theta_0| \sim 10^{-2}$  in the vicinity of the QCD phase transition. Naively, this small numerical factor  $|\theta/\theta_0| \sim 10^{-2}$  may lead only to minor effects  $\sim 10^{-2}$ . However, the crucial point is that, while the coupling (18) of the axion background field with quarks is indeed relatively small on the QCD scales, it is nevertheless effectively long ranged and long lasting, in contrast with conventional QCD interactions. As a result, this coherent  $CP$ -odd coupling may produce large effects of order of 1, as we argue below.

Indeed, as we discussed in Sec. VI, a typical oscillation time  $t_{\text{osc}}$  when the baryon charge accretes on the wall is of

order  $t_{\text{osc}} \sim m_a^{-1}$  according to Eq. (52). But this time scale  $t_{\text{osc}} \sim m_a^{-1}$  is precisely the time scale when  $\dot{\theta} = m_a(t)$  varies according to (58). Therefore, while the dynamical fermion fields  $\theta_1, \theta_2$  defined by (16) fluctuate with typical scale of order  $\Lambda_{\text{QCD}} \gg m_a$ , the coherent variation of these fields will occur during a long (on the QCD scales) coherent process when a nugget makes a single cycle. These coherent corrections are expected to be different for nuggets (positive  $\mu$ ) and antinuggets (negative  $\mu$ ) as a result of many  $C$  and  $CP$ -violating effects such as scattering, transmission, reflection, annihilation, evaporation, mixing of the scalar and pseudoscalar condensates, etc., which are all responsible for the accretion of the baryon charge on a nugget during its long evolution.

An important comment here is that each quark experiences a small difference in interacting with the domain wall surrounding nuggets or antinuggets during every single QCD event (mentioned above) with typical QCD time scale  $\Lambda_{\text{QCD}}^{-1}$ . However, the number of the coherent QCD events  $n_{\text{coherent}}$  during a long single cycle is very large,

$$n_{\text{coherent}} \sim \Lambda_{\text{QCD}} t_{\text{osc}} \sim \frac{\Lambda_{\text{QCD}}}{m_a} \sim 10^{10} \gg 1. \quad (59)$$

Therefore, a net effect during every single cycle will be order of 1, in spite of the fact that each given QCD event is proportional to the axion field  $\theta(t)$  and could be quite small.

The argument presented above holds as long as the axion field remains coherent; see also a comment at the very end of this subsection. In other words, a small but nonvanishing coherent  $CP$ -violating parameter  $\theta(t)$  plays the role of catalyst, which determines a preferred direction for the separation of the baryon charges on the Universe scale; see the few comments in Sec. III on the justification of this assumption. This role of  $CP$  violation in our framework is very different from conventional ‘‘baryogenesis’’ mechanisms when a  $CP$ -violating parameter explicitly enters the final expression for the baryon charge production.

The corresponding large coherent corrections during a single cycle  $t_{\text{osc}}$  imply that the fast fluctuating fields  $\theta_1, \theta_2$  [which effectively describe the dynamics of the fermions living on the wall according to (16)] receive large corrections during every single cycle,

$$\Delta\theta_1(t) \sim \Delta\theta_2(t) \sim 1. \quad (60)$$

These changes of order 1 of the strongly interacting  $\theta_1, \theta_2$  fields lead to modification of the accreted baryon charge per single cycle per single degree of freedom,

$$\Delta N \sim (\Delta\theta_1 + \Delta\theta_2) \sim 1, \quad (61)$$

on the nuggets according to (20). One should emphasize that the corrections (61) are expected to be different for nuggets and antinuggets because the interaction (56), (18) which is responsible for these corrections (61) breaks the

symmetry between nuggets and antinuggets when  $\mu \rightarrow -\mu$ , as discussed above.

Precise computations of these coherent  $CP$ -violating effects are hard to carry out explicitly as they require a solution of many-body problem of the coherent wall fermions with surrounding environment in the background of the axion field (57) when a large number of  $C$  and  $CP$ -violating effects take place and drastically modify the evolution of nuggets vs antinuggets. A large number of cycles of every individual nugget (antinugget) also introduces a huge uncertainty in computations of  $\Delta N$  during the time evolution when a single cycle leads to the effect of order 1, with a possible opposite sign for a consequent cycle. In other words, it is very hard to predict what would be the final outcome of the system after a large number of cycles when each cycle produces the effect of order 1. We expect that the final result would be again of order 1. Such a computation is beyond the scope of the present work. Therefore, in what follows, we introduce a phenomenological parameter  $c(T)$  of order 1 to account for these effects. All the observables will be expressed in terms of this single phenomenological parameter  $c(T) \sim 1$ ; see Eq. (62).

Our final comment in this subsection is as follows. The charge separation effect on the largest possible scales is only possible when the axion field (57) is coherent on the scales of the Universe. This coherence is known to occur in conventional studies on the dynamics of the axion field in the vicinity of the QCD phase transition if the PQ phase transition occurs before inflation; see the few comments in Sec. III on this matter. At the same time, soon after the QCD phase transition, the dominant part of the axion field transfers its energy to the free propagating on-shell axions (which is the subject of axion search experiments [8–13,15]). These randomly distributed free axions are not in the coherent state anymore. Therefore, the coherent accumulation effect which leads to a preferential formation of one species of nuggets, as discussed above, ceases to be operational at the moment of decoherence  $t_{\text{dec}}$  when the description in terms of the coherent axion field (57) breaks down.<sup>13</sup> The baryon asymmetry we observe today in this framework is a result of accumulation of the charge separation effect from the beginning of the nugget's formation until this very last ‘‘freeze-out’’ moment determined by  $t_{\text{dec}}$ .

## B. Nuggets vs antinuggets on the large scale: Generic consequences

As we already mentioned, to make any precise dynamical computations of  $\Delta N \sim 1$  due to the coherent axion

<sup>13</sup>The decoherence time  $t_{\text{dec}}$  is not entirely determined by the absolute value of the amplitude of the axion field (57). In fact, the amplitude could be quite small, but the field remains coherent on large scales. The computation of the decoherence time  $t_{\text{dec}}$  is a hard problem of Quantum field theory (QFT), similar to a problem in quantum optics when initially coherent light becomes a decoherent superposition of uncorrelated photons.

field (57) is a hard problem of strongly coupled QCD at  $\theta \neq 0$ . To effectively account for these coherent effects, one can introduce an unknown coefficient  $c(T)$  of order 1 as

$$B_{\text{antinuggets}} = c(T) \cdot B_{\text{nuggets}}, \quad \text{where } |c(T)| \sim 1, \quad (62)$$

where  $c(T)$  is obviously a negative constant of order 1. We emphasize that the main claim of this section represented by Eq. (62) is not very sensitive to the axion mass  $m_a(T)$  nor to the magnitude of  $\theta(T)$  at the QCD phase transition when the bubbles start to oscillate and slowly accrete the baryon charge. The only crucial factor in our arguments is that the typical variation of  $\theta(t)$  is determined by the axion mass (58), which is the same order of magnitude as  $t_{\text{osc}}^{-1}$ , and furthermore this variation is correlated on the scale where the axion field (57) can be represented by the coherent superposition of the axions at rest.

The key relation of this framework (62) unambiguously implies that the baryon charge in the form of the visible matter can be also expressed in terms of the same coefficient  $c(T) \sim 1$  as follows:

$$B_{\text{visible}} = -B_{\text{antinuggets}} - B_{\text{nuggets}}. \quad (63)$$

Using Eq. (62), it can be rewritten as

$$\begin{aligned} B_{\text{visible}} &\equiv (B_{\text{baryons}} + B_{\text{antibaryons}}) \\ &= -[1 + c(T)]B_{\text{nuggets}} \\ &= -\left[1 + \frac{1}{c(T)}\right]B_{\text{antinuggets}}. \end{aligned} \quad (64)$$

The same relation can be also represented in terms of the measured observables  $\Omega_{\text{visible}}$  and  $\Omega_{\text{dark}}$  at later times when only the baryons (and not antibaryons) contribute to the visible component,<sup>14</sup>

$$\Omega_{\text{dark}} \simeq \left(\frac{1 + |c(T)|}{|1 + c(T)|}\right) \cdot \Omega_{\text{visible}} \quad \text{at } T \leq T_{\text{form}}. \quad (65)$$

One should emphasize that the relation (64) holds as long as the thermal equilibrium is maintained, which we assume to be the case. Another important comment is that each individual contribution  $|B_{\text{baryons}}| \sim |B_{\text{antibaryons}}|$  entering (64) is many orders of magnitude greater than the baryon charge hidden in the form of the nuggets and antinuggets at earlier times when  $T_c > T > T_{\text{form}}$ . It is just their total

<sup>14</sup>In Eq. (65), we neglect the differences (due to different gaps) between the energy per baryon charge in the hadronic and CS phases to simplify notations. The corresponding corrections in energy per baryon charge in the hadronic and CS phases, in principle, can be explicitly computed from the first principles. However, we ignore these modifications in the present work. This correction obviously does not change the main claim of this proposal stating that  $\Omega_{\text{visible}} \approx \Omega_{\text{dark}}$ .

baryon charge which is labeled as  $B_{\text{visible}}$ , and representing the net baryon charge of the visible matter is the same order of magnitude (at all times) as the net baryon charge hidden in the form of the nuggets and antinuggets according to (63).

The baryons continue to annihilate each other (as well as the baryon charge hidden in the nuggets) until the temperature reaches  $T_{\text{form}}$  when all visible antibaryons get annihilated, while visible baryons remain in the system and represent the visible matter we observe today. It corresponds to  $c(T_{\text{form}}) \simeq -1.5$  as estimated below if one neglects the differences in gaps in the CS and hadronic phases; see footnote 14. After this temperature, the nuggets essentially assume their final form and do not lose or gain much of the baryon charge from outside. The rare events of the annihilation between antinuggets and visible baryons continue to occur. In fact, the observational excess of radiation in different frequency bands, reviewed in Sec. II, is a result of these rare annihilation events at the present time.

The generic consequence of this framework represented by Eqs. (62), (64), and (65) takes the following form at this time  $T_{\text{form}}$  for  $c(T_{\text{form}}) \simeq -1.5$ , which corresponds to the case when the nuggets saturate the entire dark-matter density,

$$\begin{aligned} B_{\text{visible}} &\simeq \frac{1}{2}B_{\text{nuggets}} \simeq -\frac{1}{3}B_{\text{antinuggets}}, \\ \Omega_{\text{dark}} &\simeq 5 \cdot \Omega_{\text{visible}}, \end{aligned} \quad (66)$$

which is identically the same relation (2) presented in the Introduction. The relation (66) emerges due to the fact that all components of matter, visible and dark, are proportional to one and the same dimensional parameter  $\Lambda_{\text{QCD}}$ ; see footnote 14 with a comment on this approximation. In formula (66),  $B_{\text{nuggets}}$  and  $B_{\text{antinuggets}}$  contribute to  $\Omega_{\text{dark}}$ , while  $B_{\text{visible}}$  obviously contributes to  $\Omega_{\text{visible}}$ . The coefficient  $\sim 5$  in relation  $\Omega_{\text{dark}} \simeq 5 \cdot \Omega_{\text{visible}}$  is obviously not universal, but relation (1) is universal and a very generic consequence of the entire framework, which was the main motivation for the proposal [3,4].

For example, if  $c(T_{\text{form}}) \simeq -2$ , then the corresponding relation (65) between the dark matter and the visible matter would assume the form  $\Omega_{\text{dark}} \simeq 3 \cdot \Omega_{\text{visible}}$ . Such a relation implies that there is plenty of room for other types of dark matter to saturate the observed ratio  $\Omega_{\text{dark}}^{\text{observed}} \simeq 5 \cdot \Omega_{\text{visible}}^{\text{observed}}$ . This comment will be quite important in our discussions in Sec. VIII, where we comment on implications of this framework for other axion search experiments.

One should emphasize once again that the generic consequences of the framework represented by (1) and (65) are not sensitive to any specific parameters such as the efficiency of the domain wall production or the magnitude of  $\theta$  at the QCD phase transition, which could be quite small; see footnote 13 for few comments on that. Nevertheless, precisely the coupling with the coherent  $CP$ -odd axion field plays a crucial role in the generation

of  $|c(T)| \neq 1$ ; i.e., the axion plays the role of catalyst in the baryon charge separation effect on the largest possible scales. Some other observables which are sensitive to the dynamical characteristics (e.g., the efficiency of the domain wall production) will be discussed below.

### C. $n_B/n_\gamma$ ratio: Model dependent estimates

The time evolution of the dark matter within this framework is amazingly simple. The relations (62), (63), and (64) hold at all times. The baryon charge of the nuggets (antinuggets) vary until its radius  $R(T)$  assumes its equilibrium value as described in Secs V and VI. It happens approximately at the time when the CS phase forms in the interior of the nuggets, which can be estimated as  $T_{CS} \approx 0.6\Delta \approx 60$  MeV, where  $\Delta \approx 100$  MeV is the gap of the CS phase. After this temperature, the nuggets essentially assume their final form, with very little variation in size (and baryon charge). The rare events of the annihilation of course continue to occur even for lower temperatures. In fact, the observational consequences reviewed in Sec. II are a result of these annihilation events at the present time.

The variation of the visible matter  $B_{\text{visible}}$  demonstrates much more drastic changes after the QCD phase transition at  $T_c$  because the corresponding number density is proportional to  $\exp(-m_N/T)$  such that at the moment of formation  $T_{\text{form}} \approx 40$  MeV the baryon-to-entropy ratio assumes its present value (5), which we express as follows:

$$\eta \equiv \frac{n_B}{n_\gamma} \approx \frac{B_{\text{visible}}/V}{n_\gamma} \sim 10^{-10}, \quad n_B \equiv \frac{B_{\text{visible}}}{V}. \quad (67)$$

If the nuggets and antinuggets were not present at this temperature, the conventional baryons and antibaryons would continue to annihilate each other until the density would be 9 orders of magnitude smaller than observed (67) when the temperature would be around  $T \approx 22$  MeV. Conventional baryogenesis resolves this ‘‘annihilation catastrophe’’ by producing extra baryons in early times; see, e.g., Ref. [19], while in our framework, extra baryons and antibaryons are hidden in form of the macroscopically large nuggets.

In our framework, the ratio (67) can be rewritten in terms of the nugget's density as the baryon charges in the form of the visible matter and in the form of the nuggets are related to each other according to (64). This relation allows us to infer what efficiency is required for the bubbles to form and survive until the present time when the observed ratio is measured (67).

One should emphasize that any small factors which normally enter the computations in conventional baryogenesis (such as  $C$ - and  $CP$ -violating parameters) do not enter in the estimates presented below in our framework as a result of two effects. First, the  $C$  violation enters the computation as a result of generation of the chemical

potential  $\mu$  as described in Sec. IV. It is expressed in terms of spontaneous accretion of the baryon charge on the surface of the nuggets as given by Eq. (20), which effectively generates the chemical potential (33), which can be thought of as the local violation of the symmetry on the scale of a single nugget. Second, the  $CP$  violation enters the computation in the form of the coupling with the coherent axion field (56). Precisely this coupling as we argued above leads to removing of the degeneracy between nuggets and antinuggets formally expressed as  $c(T) \sim 1$  in Eq. (62). Therefore, the only small parameter we anticipate in our estimates below is due to some suppression of the closed bubbles which must be formed with sufficiently large sizes during the QCD phase transition.

We cannot compute the probability for the bubble formation as it obviously requires the numerical simulations, which is beyond the scope of the present work. Instead, we go backward and ask the question of what the efficiency of the bubble formation at the QCD phase transition should be in order to accommodate the observed ratio (67).

With these comments in mind, we proceed with our estimates as follows. First, from (64) and (66), we infer that the baryon charge hidden in the nuggets and antinuggets is the same order of magnitude as the baryon charge of the visible baryons at  $T_{\text{form}}$  at the end of the formation, i.e.,

$$\frac{B_{\text{nuggets}}/V}{n_\gamma} \gtrsim 10^{-10}, \quad (68)$$

where we use sign  $\gtrsim$  instead of  $\approx$  used in Eq. (67) to emphasize that there is long time for equilibration between the moment  $T_{CS} \approx 0.6\Delta \approx 60$  MeV when the CS phase forms in the interior of the nuggets and  $T_{\text{form}} \approx 40$  MeV when all antibaryons of the visible matter get annihilated, corresponding to the present observed value (67). During this period, the equilibrium between the visible matter and the baryons from nuggets is maintained, and some portion of the nugget's baryon charge might be annihilated by the visible matter. This explains our sign  $\gtrsim$  used in Eq. (68).

The relation (68) implies that the number density of nuggets and antinuggets can be estimated as

$$\frac{\langle B \rangle n_{\text{nuggets}}}{n_\gamma} \gtrsim 10^{-10}, \quad \langle B \rangle n_{\text{nuggets}} \equiv \frac{B_{\text{nuggets}}}{V}, \quad (69)$$

where  $\langle B \rangle$  is the average baryon charge of a single nugget at  $T_{\text{form}}$ .

Now, we want to estimate the same ratio (69) using the KZ mechanism [40–42] reviewed in Sec. III. The basic idea of the KZ mechanism is that the total area of the crumpled, twisted, and folded domain wall is proportional to the volume of the system and can be estimated as

$$S_{(\text{total DW})} = \frac{V}{\xi(T)}, \quad (70)$$

where  $\xi(T)$  is the correlation length, which is defined as an average distance between crumpled domain walls at temperature  $T$ . The largest part of the wall belongs to the percolated large cluster. It is known that some closed walls (bubbles) with typical size  $\xi(T)$  will be also formed. These bubbles with sufficiently large size  $R \sim \xi(T)$  will eventually become nuggets. We introduce parameter  $\gamma$  to account for the suppression related to the closed bubble formation. In other words, we define

$$S_{\text{nuggets}} = \gamma S_{(\text{total DW})} = \frac{\gamma V}{\xi(T)}, \quad \gamma \ll 1. \quad (71)$$

At the same time, the total area of the nuggets  $S_{\text{nuggets}}$  can be estimated as

$$S_{\text{nuggets}} = 4\pi R_0^2(T) [V \cdot n_{\text{nuggets}}], \quad (72)$$

where  $R_0$  is the size of a nuggets at the initial time, while  $[V \cdot n_{\text{nuggets}}]$  represents the total number of nuggets in volume  $V$ . Comparison (71) with (72) gives the following estimate for the nugget's density when bubbles just formed:

$$n_{\text{nuggets}} \simeq \frac{\gamma}{4\pi R_0^2 \xi}. \quad (73)$$

The last step in our estimates is the computation of the average baryon charge of a nugget at  $T_{\text{CS}}$  when CS sets in inside the nugget. The corresponding estimates were worked out long ago [3] and reproduced in Sec. V in the course of the time evolution by taking  $t \rightarrow \infty$ ; see (34). The baryon number density inside the nuggets depends on a model being used [3], but typically it is a few times the nuclear saturation density  $n_0 \simeq (108 \text{ MeV})^3$ , which is consistent with conventional computations for the baryon density in CS phases. Therefore, we arrive at

$$\langle B \rangle \simeq (2 - 6)n_0 \cdot \frac{4\pi R_{\text{form}}^3}{3}, \quad (74)$$

where  $R_{\text{form}}$  is the final size of the nuggets. By substituting (74) and (73) into (69), we arrive at the constraint on the efficiency of the bubble formation represented by parameter  $\gamma$ ,

$$(2 - 6) \cdot \frac{\gamma}{3} \left( \frac{R_{\text{form}}}{\xi(T)} \right) \left( \frac{R_{\text{form}}}{R_0} \right)^2 \left( \frac{n_0}{n_\gamma} \right) \gtrsim 10^{-10}, \quad (75)$$

where the expression for  $n_\gamma(T)$  should be taken at the formation time,

$$n_\gamma = \frac{2\zeta(3)}{\pi^2} T_{\text{form}}^3, \quad \zeta(3) \simeq 1.2, \quad (76)$$

while the correlation length  $\xi(T)$  should be evaluated at much earlier times, close to  $T_c$  when the domain wall

network only started to form. Typically, bubbles form with  $R_0 \sim \xi$ . However, the bubbles shrink approximately 3–5 times according to (51) before they reach equilibrium during the time evolution as discussed in Sec. VI. Therefore, to be on the safe side, we make the very conservative assumption that

$$\frac{R_{\text{form}}}{R_0} \sim 0.1, \quad R_0 \simeq \xi. \quad (77)$$

To proceed with numerical estimates, it is convenient to separate  $\gamma$  on two pieces,

$$\gamma \equiv \gamma_{\text{formation}} \cdot \gamma_{\text{evolution}}, \quad \gamma_{\text{formation}} \sim 0.1, \quad (78)$$

where the first part,  $\gamma_{\text{formation}} \sim 0.1$ , has been estimated using numerical simulations; see Ref. [42] for a review. The second suppression factor  $\gamma_{\text{evolution}}$  is unknown and includes a large number of different effects. In particular, many small closed bubbles with  $R_0 \leq \xi$  are very likely to be formed but may not survive the evolution, as we discussed in Sec. VI. Furthermore, there are many effects such as evaporation and annihilation inside the nuggets, which may also lead to the collapse of relatively small nuggets. Furthermore, the formation probability of large closed bubbles with  $R_0 \gg \xi$  (which are most likely to survive) is highly suppressed  $\sim \exp(-R_0^2/\xi^2)$ . All these effects are included in unknown parameter  $\gamma_{\text{evolution}}$ . Our constraint (from observations on  $n_B/n_\gamma$  within our mechanism) can be inferred from (75)

$$\gamma_{\text{evolution}}(T_{\text{form}}) \gtrsim 10^{-7}. \quad (79)$$

One suppression factor which obviously contributes to suppression (79) is related to the necessity to produce a sufficiently large initial bubble for successful nugget formation as given by Eq. (51).

Now, we can interpret the estimate (79) in two complementary ways.<sup>15</sup> First, the interpretation of estimate (79) is as follows. Small numerical value (79) implies that only sufficiently large nuggets survive the evolution in the unfriendly environment mentioned above. It is hard to estimate all the QCD effects mentioned above (evaporation, annihilation inside the nuggets, etc.), but the dominant suppression factor is related to formation suppression  $\sim \exp(-R_0^2/\xi^2)$ . The observed abundance (67) can be interpreted in this case as a specific value for the formation size  $R_0$  which satisfies the constraint (79). There is an exponential sensitivity to  $R_0$  within this interpretation. In particular, if  $R_0 \sim (3 - 4)\xi$ ,

<sup>15</sup>We are thankful to an anonymous referee, who hinted at the possibility of the first interpretation. The second interpretation of estimate (79) is our original and preferable interpretation.

$$\exp\left(-\frac{R_0^2}{\xi^2}\right) \sim (10^{-4} - 10^{-7}). \quad (80)$$

This estimate is consistent with the observational constraint as the unaccounted-for QCD effects mentioned above may saturate (79).

We do not consider this sensitivity to  $R_0$  as a fine-tuning problem. Indeed, in many cases, the physics is highly sensitive to some parameters of the theory, which, however, cannot be interpreted as a fine-tuning problem. In particular, in the context of this paper, the conventional formula (81) for the dark-matter density that resulted from the misalignment mechanism is highly sensitive to the axion mass  $m_a$ . However, we do not interpret this dependence as a fine-tuning problem.

Our second (and preferable) interpretation can be explained as follows. The observed ratio (67) is highly sensitive to  $T_{\text{form}} \approx 40$  MeV due to the exponential dependence of the baryon number density  $\sim \exp(-m_N/T)$ . This formation temperature in our framework is defined as the temperature when the nuggets complete their formation. This value for the temperature is very reasonable as it lies slightly below  $T_{\text{CS}}$  when the CS phase sets in inside the nuggets. Obviously, we do not interpret this sensitivity to the formation temperature  $T_{\text{form}} \approx 40$  MeV as a fine-tuning problem.

The crucial point here is that the saturation of the observed ratio (67) can be interpreted in terms of  $T_{\text{form}}$ , or it can be interpreted in terms of  $R_0$ , which is the key parameter in our first interpretation. A small variation of  $T_{\text{form}}$  can be thought of as small variations of  $R_0$ , which, however, lead to very large changes of the observed ratio (67) due to the exponential sensitivity. In other words, a small increase of  $T_{\text{form}}$  when nuggets complete the formation can be interpreted as a small decrease of survival size  $R_0$  in our first interpretation given above.

We do not call this effect a fine-tuning. This is because the equilibration of the baryon charge from the nuggets with visible baryons always leads to generic relations (1), (64). These relations are the direct consequence of our framework when all contributions are the same orders of magnitude. A small observed ratio (67) is determined by a precise and specific moment in evolution of the Universe when the nuggets complete their formation at temperature  $T_{\text{form}} \sim \Lambda_{\text{QCD}}$ , which is again perfectly consistent with the main paradigm of the entire framework that all dimensional parameters are of order  $\Lambda_{\text{QCD}}$ . This  $T_{\text{form}}$  corresponds to a very specific value  $R_0$  for nuggets to complete their formation at time  $T_{\text{form}}$ .

How can one understand the result (79), which essentially states that even a very tiny probability of the formation of the closed bubbles is still sufficient to saturate the observed ratio (67)? The answer lies in the observation that the baryon density  $n_B \approx n_{\bar{B}}$  was 10 orders of magnitude larger at the moment of the bubble formation. Therefore, even a tiny

probability at the moment of formation of a closed bubble with sufficiently large size will lead to effects of order 1 at the moment when the baryon number density drops 10 orders in magnitude. Another reason why a very tiny probability of the formation of the closed bubbles nevertheless is sufficient to saturate the observed ratio (67) is that typical ‘‘small factors’’ which normally accompany the conventional baryogenesis mechanisms such as  $CP$ - and  $C$ -odd couplings do not appear in estimate (79) due to the reasons already explained after Eq. (67).

We conclude this section with the following comment: The basic consequences of this framework represented by Eqs. (1), (64), and (65) are very generic. These features are not very sensitive to the efficiency of the closed domain wall formation nor to the absolute value of  $\theta$  as long as coherence is maintained; see footnote 13. These generic features hold for an arbitrary value of the axion mass  $10^{-6} \text{ eV} \leq m_a \leq 10^{-3} \text{ eV}$ , in contrast with the conventional treatment of the axion as the dark-matter candidate, when  $\Omega_{\text{DM}}$  can be saturated by the axions only when the axion mass assumes a very specific and definite value  $m_a \approx 10^{-6} \text{ eV}$ ; see the next section for details.

The derivation of the observed ratio (67) from the first principles (which is determined by parameter  $R_0$  in the first interpretations or parameter  $T_{\text{form}}$  in the second interpretation) is a hard computational problem of strongly coupled QCD when all elements such as the cooling rate, annihilation rate, charge separation rate, damping rate, evaporation rate, and many other effects equally contribute to  $T_{\text{form}}$ . However, it is important that the ‘‘observational’’ value  $T_{\text{form}} \approx 40$  MeV lies precisely in the region where it should be,  $T_{\text{form}} < T_{\text{CS}}$ , i.e., slightly below the temperature at which CS sets in. Therefore, any fine-tuning procedures have never been required in this framework to accommodate the observed ratio presented by Eq. (1).

## VIII. IMPLICATIONS FOR THE AXION SEARCH EXPERIMENTS

The goal of this section is to comment on the relation of our framework and the direct axion search experiments [8–15]. We start with the following comment we made in Sec. II: This model which has a single fundamental parameter (a mean baryon number of a nugget  $\langle B \rangle \sim 10^{25}$  entering all the computations) is consistent with all known astrophysical, cosmological, satellite, and ground-based constraints as reviewed in Sec. II. For discussions of this section, it is convenient to express this single normalization parameter  $\langle B \rangle \sim 10^{25}$  in terms of the axion mass  $m_a \sim 10^{-4} \text{ eV}$  as these two parameters are directly related according to the scaling relations (3). The corresponding relation between these two parameters occurs because the axion mass  $m_a$  determines the wall tension  $\sigma \sim m_a^{-1}$  which itself enters the expression for the equilibrium value of the size of the nuggets,  $R_{\text{form}}$ , at the end of the formation.

One should emphasize that it is quite nontrivial that the cosmological constraints on the nuggets as shown on Fig. 2 and formulated in terms of  $\langle B \rangle$  are compatible with known upper limit on the axion mass  $m_a < 10^{-3}$  eV within our framework. One could regard this compatibility as a non-trivial consistency check for this proposal.

The lower limit on the axion mass, as it is well known, is determined by the requirement that the axion contribution to the dark-matter density does not exceed the observed value  $\Omega_{\text{dark}} \approx 0.23$ . There are a number of uncertainties in the corresponding estimates. We shall not comment on these subtleties by referring to the review papers [8–15]. The corresponding uncertainties are mostly due to the remaining discrepancies between different groups on the computations of the axion production rates due to the different mechanisms such as the misalignment mechanism vs domain wall/string decays. In what follows, to be more concrete in our estimates, we shall use the following expression for the dark-matter density in terms of the axion mass resulting from the misalignment mechanism [15]:

$$\Omega_{(\text{DM axion})} \approx \left( \frac{6 \times 10^{-6} \text{ eV}}{m_a} \right)^{\frac{7}{6}}. \quad (81)$$

This formula essentially states that the axion of mass  $m_a \approx 2 \times 10^{-5}$  eV saturates the dark-matter density observed today, while the axion mass in the range of  $m_a \geq 10^{-4}$  eV contributes very little to the dark-matter density. This claim, of course, is entirely based on estimate (81), which accounts only for the axions directly produced by the misalignment mechanism suggested originally in Ref. [44].

There is another mechanism of the axion production when the Peccei-Quinn symmetry is broken after inflation. In this case, the string-domain wall network produces a large number of axions such that the axion mass  $m_a \approx 10^{-4}$  eV may saturate the dark-matter density; see relatively recent estimates [43,46,59] with some comments and references in previous papers. The corresponding formula from Refs. [43,46,59] is also highly sensitive to the axion mass with  $m_a$  dependence being very similar to Eq. (81).

The main lesson to be learned from the present work is that, in addition to these well-established mechanisms previously discussed in the literature, there is an additional contribution to the dark-matter density also related to the axion field. However, the mechanism which is advocated in the present work contributes to the dark-matter density through the formation of the nuggets, rather than through the direct axion production. The corresponding mechanism as argued in Sec. VII B always satisfies the relation  $\Omega_{\text{dark}} \approx \Omega_{\text{visible}}$  and, in principle, is capable of saturating the dark-matter density  $\Omega_{\text{dark}} \approx 5\Omega_{\text{visible}}$  by itself for an arbitrary magnitude of the axion mass  $m_a$  as the corresponding contribution is not sensitive to the axion mass, in contrast with conventional mechanisms mentioned above. A precise

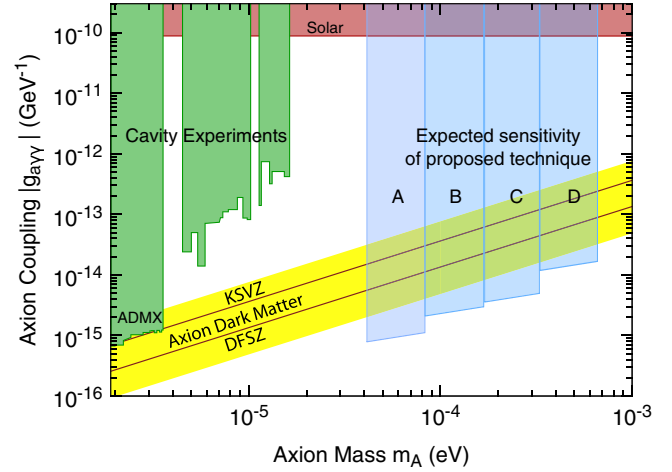


FIG. 3. Cavity/ADMX experimental constraints on the axion mass are shown in green. The expected sensitivity for the Orpheus axion search experiment [14] is shown by blue regions A, B, C, and D. In particular, experiment B, covers the most interesting region of the parametrical space with  $m_a \approx 10^{-4}$  eV corresponding to the nuggets with mean baryon charge  $\langle B \rangle \approx 10^{25}$  which itself satisfies all known astrophysical, cosmological, satellite, and ground-based constraints; see Fig. 2. The plot is taken from Ref. [14].

coefficient in ratio  $\Omega_{\text{dark}} \approx \Omega_{\text{visible}}$  is determined by a parameter of order 1,  $|c(T)| \sim 1$ , which unfortunately is very hard to compute from the first principles, as discussed in Sec. VII B.

Our choice for  $m_a \approx 10^{-4}$  eV which corresponds to  $\langle B \rangle \sim 10^{25}$  is entirely motivated by our previous analysis of astrophysical, cosmological, satellite, and ground-based constraints, as reviewed in Sec. II. As we mentioned in Sec. II, there are a number of frequency bands for which some excess of emission was observed, and this model may explain some portion, or even the entire excess, of the observed radiation in these frequency bands. Our normalization  $\langle B \rangle \sim 10^{25}$  was fixed by Eq. (6) with the assumption that the observed dark matter is saturated by the nuggets. Relaxing this assumption obviously modifies the coefficient  $c(T)$  as well as  $\langle B \rangle$ .

Interestingly enough, this range of the axion mass  $m_a \approx 10^{-4}$  eV is perfectly consistent with the recent claim [60,61] that the previously observed small signal in the resonant S/N/S Josephson junction [62] is a result of the dark-matter axions with the mass  $m_a \approx 1.1 \times 10^{-4}$  eV. Furthermore, it has been also claimed that similar anomalies have been observed in other experiments [63–65] which all point toward an axion mass  $m_a \approx 1.1 \times 10^{-4}$  eV if interpreted within the framework [60,61]. The only comment we would like to make here is that if the interpretation [60,61] of the observed anomalies [62–65] is indeed due to the dark-matter axions then the corresponding axion mass is perfectly consistent with our estimates (based on cosmological observations) of the

average baryon charge of the nuggets  $\langle B \rangle \simeq 10^{25}$  as reviewed in Sec. II.

We conclude this section on an optimistic note with a remark that the most interesting region of the parametric space corresponding to the nuggets with mean baryon charge  $\langle B \rangle \simeq 10^{25}$  might be tested by the Orpheus axion search experiment [14] as shown in Fig. 3.

## IX. CONCLUSION: FUTURE DIRECTIONS

First, we want to list the main results of the present studies, while comments on possible future developments will be presented at the end of this Conclusion:

- (1) The first key element of this proposal is the observation (20) that the closed axion domain walls are copiously produced and generically will acquire the baryon or antibaryon charge. This phenomenon of the separation of the baryon charge can be interpreted as a local version of spontaneous symmetry breaking. This symmetry breaking occurs not in the entire volume of the system but on the correlation length  $\xi(T) \sim m_a^{-1}$ , which is determined by the folded and crumpled axion domain wall during the formation stage. Precisely this local charge separation eventually leads to the formation of the nuggets and antinuggets serving in this framework as the dark-matter component  $\Omega_{\text{dark}}$ .
- (2) The number density of nuggets and antinuggets will not be identically the same as a result of the coherent (on the scale of the Universe) axion  $CP$ -odd field. We parametrize the corresponding effects of order 1 by phenomenological constant  $c(T) \sim 1$ . It is important to emphasize that this parameter of order 1 is not a fundamental constant of the theory but calculable from the first principles. In practice, however, such a computation could be quite a challenging problem when even the QCD phase diagram is not known. The fundamental consequence of this framework,  $\Omega_{\text{dark}} \approx \Omega_{\text{visible}}$ , which is given by (1) is *universal* and not sensitive to any parameters as both components are proportional to  $\Lambda_{\text{QCD}}$ . The observed ratio (2), (66) corresponds to a specific value of  $c(T_{\text{form}}) \simeq -1.5$ , as discussed in Sec. VII B.
- (3) Another consequence of the proposal is a natural explanation of the ratio (5) in terms of the formation temperature  $T_{\text{form}} \simeq 40$  MeV, rather than in terms of specific coupling constants which normally enter conventional baryogenesis computations. This observed ratio is expressed in our framework in terms of a single parameter  $T_{\text{form}}$  when nuggets complete their formation. This parameter is not a fundamental constant of the theory and, as such, is calculable from the first principles. In practice, however, the computation of  $T_{\text{form}}$  is quite a challenging problem, as explained in Sec. VII C. Numerically, the observed ratio (5) corresponds to  $T_{\text{form}} \simeq 40$  MeV,

which is indeed slightly below the critical temperature  $T_{\text{CS}} \simeq 60$  MeV where the color superconductivity sets in.

The relation  $T_{\text{form}} \lesssim T_{\text{CS}} \sim \Lambda_{\text{QCD}}$  is universal in this framework as both parameters are proportional to  $\Lambda_{\text{QCD}}$ . As such, the universality of this framework is similar to the universality  $\Omega_{\text{dark}} \approx \Omega_{\text{visible}}$  mentioned in the previous item. At the same time, the ratio (5) is not universal itself as it is exponentially sensitive to precise value of  $T_{\text{form}}$  due to the conventional suppression factor  $\sim \exp(-m_p/T)$ .

- (4) The only new fundamental parameter of this framework is the axion mass  $m_a$ . Most of our computations (related to the cosmological observations; see Sec. II and Fig. 2), however, are expressed in terms of the mean baryon number of nuggets  $\langle B \rangle$  rather than in terms of the axion mass. However, these two parameters are unambiguously related according to the scaling relations (3). Our claim is that all universal properties of this framework listed above still hold for any  $m_a$ . In other words, there is no fine-tuning in the entire construction with respect to  $m_a$ . The constraints (and possible cosmological observations) from Sec. II strongly suggest  $\langle B \rangle \simeq 10^{25}$ , which can be translated into the preferred value for the axion mass  $m_a \simeq 10^{-4}$  eV.
- (5) This region of the axion mass  $m_a \simeq 10^{-4}$  eV corresponding to the average size of the nuggets  $\langle B \rangle \simeq 10^{25}$  can be tested in the Orpheus axion search experiment [14] as shown on Fig. 3.

We conclude with few thoughts on future directions within our framework. It is quite obvious that future progress cannot be made without a much deeper understanding of the QCD phase diagram at  $\theta \neq 0$ . In other words, we need to understand the structure of possible phases along the third dimension parametrized by  $\theta$  in Fig 1.

Presently, very few results are available regarding the phase structure at  $\theta \neq 0$ . First of all, the phase structure is understood in a simplified version of QCD with two colors,  $N_c = 2$  at  $T = 0$ ,  $\mu \neq 0$ ; see Ref. [66]. In fact, the studies [66] were mostly motivated by the subject of the present work and related to the problem of the formation of the quark nuggets during the QCD phase transition in early Universe with nonvanishing  $\theta$ . With few additional assumptions, the phase diagram can be also conjectured for the system with large number of colors  $N_c = \infty$ , at nonvanishing  $T$ ,  $\mu$ ,  $\theta$ ; see Refs. [67,68].

Because of the known ‘‘sign problem,’’ see footnote 1, the conventional lattice simulations cannot be used at  $\theta \neq 0$ . The corresponding analysis of the phase diagram for nonvanishing  $\theta$  started just recently by using some newly invented technical tricks [69–72].

Another possible development from the ‘‘wish list’’ is a deeper understanding of the closed bubble formation.

Presently, very few results are available on this topic. The most relevant for our studies is the observation made in Ref. [10] that a small number of closed bubbles are indeed observed in numerical simulations. However, their detail properties (their fate, size distribution, etc.) have not been studied yet. A number of related questions such as an estimation of correlation length  $\xi(T)$ , the generation of the structure inside the domain walls, the baryon charge accretion on the bubble, etc., hopefully can be also studied in such numerical simulations.

One more possible direction for future studies from the wish list is a development some QCD-based models where a number of hard questions such as the evolution of the nuggets, cooling rates, evaporation rates, annihilation rates, viscosity of the environment, transmission/reflection coefficients, etc., in an unfriendly environment with nonvanishing  $T$ ,  $\mu$ ,  $\theta$  can be addressed, and hopefully answered. All these and many other effects, in general, equally contribute to our parameters  $T_{\text{form}}$  and  $c(T)$  at the  $\Lambda_{\text{QCD}}$  scale in strongly coupled QCD. Precisely these numerical factors eventually determine the coefficients in the observed relations:  $\Omega_{\text{dark}} \approx \Omega_{\text{visible}}$  given by Eq. (65) and  $n_B/n_\gamma$  expressed by Eq. (67).

Last but not least, the discovery of the axion in the Orpheus experiment [14] would conclude a long and fascinating journey of searches for this unique and amazing particle conjectured almost 40 years ago. Such a discovery would be a strong motivation for related searches of “something else” as the axion mass  $m_a \approx 10^{-4}$  is unlikely to saturate the dark-matter density observed today. We advocate the idea that this something else is the “quark nuggets” (where the axion plays the key role in the entire construction), which could provide the principle contribution to the dark matter of the Universe as the relation  $\Omega_{\text{dark}} \approx \Omega_{\text{visible}}$  in this framework is not sensitive to the axion mass.

## ACKNOWLEDGMENTS

This work was supported in part by the National Science and Engineering Research Council of Canada.

## APPENDIX A: ESTIMATION OF FLUXES

The main goal of this Appendix is to argue that the approximation in Eq. (32), which was adopted in the text by neglecting extra term “fluxes,” is justified, at least on the qualitative level. In other words, while these flux terms are obviously present in the system, they, nevertheless, do not drastically change a key technical element [an implicit relation between  $R(t)$  and  $\mu(t)$ ] which this equation provides. Precisely this implicit relation between  $R(t)$  and  $\mu(t)$  eventually allows us to express the  $\mu$ -dependent pressure  $\Delta P[\mu]$  in terms of  $R$ -dependent function  $\Delta P[f(R)]$  such that the basic equation (45) describing the time evolution of the nuggets is reduced to a differential equation on a single variable  $R(t)$ .

Our starting point is the observation that the relevant flux which enters Eq. (32) is  $\Delta\Phi = (\Phi_{\Rightarrow} - \Phi_{\Leftarrow})$ , counting the

net baryon charge transfer and sensitive to the chemical potential difference, rather than the total flux  $\langle\Phi\rangle$  which counts the exchange of all the particles, including bosons.<sup>16</sup> In fact, if the average flux  $\langle\Phi\rangle$  were entering Eq. (32), one could explicitly check that this term would be the same order of magnitude as two other terms of the equation. However, the key point is that the baryon charge transfer  $\Delta\Phi$  is numerically suppressed, i.e.,  $\Delta\Phi \ll \langle\Phi\rangle$ . In fact,  $\Delta\Phi$  identically vanishes for  $\mu = 0$ . Furthermore, one can use the same technique which has been used in Sec. VI A to argue that  $\Delta\Phi \ll \langle\Phi\rangle$  in entire region of  $\mu$ . Numerical analysis supports this claim.

To reiterate this claim, while a typical flux defined as

$$\Phi = \frac{g^{\text{in}}}{(2\pi)^3} \int \frac{v_z d^3k}{\exp(\frac{k-\mu}{T}) + 1} + (\text{bosons}) \sim (\text{fm})^{-3} \quad (\text{A1})$$

assumes a conventional QCD value, the net baryonic flux  $\Delta\Phi \cdot S$  through surface  $S$  is numerically suppressed and can be neglected in Eq. (32).

One can explain this result as follows. Consider a single oscillation of the domain wall evolution. To be more specific, consider a squeezing portion of this evolution when  $R(t)$  decreases. During this process, the chemical potential (and the baryon charge density) locally grows as we discussed in Sec. VI A. The major portion of this growth results from the baryon charge which was already bound to the domain wall rather than from the baryon charge which enters the system as a result of the baryonic flux transfer.

On an intuitive level, the dominance of the bound charges [accounted for in Eq. (32)] in comparison with flux contribution [neglected in Eq. (32)] can be explained using pure geometrical arguments. Indeed, the chemical potential increases very fast as a result of rapid shrinking of the bubble with speed  $v \approx c$ . The corresponding contraction of a bubble leads to a proportionally rapid increase of the chemical potential on the domain wall. This happens because the baryon charges strongly bound to the wall and cannot leave the system due to the topological reasons as the boundary conditions effectively lock the charge to the macroscopically large domain wall. As a result of this evolution, the binding energy of a quark  $\sim\mu$  increases when the bubble contracts. This process represents a highly efficient mechanism of very rapid growth of the chemical potential due to the domain wall dynamics. It is very hard to achieve a similar efficiency with the flux contribution when the probability for a reflection from the domain wall is typically much higher than the probability for a

<sup>16</sup>The dominant contribution to the fluxes normally comes from the lightest degrees of freedom which are the Nambu-Goldstone bosons in the hadronic and CS phases. These contributions are crucial for maintaining the thermodynamical equilibrium between the exterior and interior, but they do not play any role in the baryon fluxes which enter Eq. (32).

transmission. Furthermore, a nonvanishing quark mass make suppression even stronger  $\sim \exp(-m/T)$ .

To conclude, we do expect that an accounting for the flux contribution modifies our equations relating  $\mu(t)$  and  $R(t)$  as expressed by Eqs. (32) and (38). However, we do not expect that this modification may drastically change the basic qualitative features of Eqs. (32) and (38), which have been heavily employed in this work.

## APPENDIX B: FORMATION OF THE NUGGETS: NUMERICAL ANALYSIS

This Appendix is devoted to exact numerical computation in contrast with analytical qualitative arguments presented in Sec. VI. The basic lesson of this Appendix is that a number of simplifications which have been made in Sec. VI are justified, at least, on a qualitative level.

Before we proceed with numerical computations, we want to make few comments on parameters entering the basic dynamical equation (45). In the previous sections,  $\sigma$  was treated as a constant in order to simplify the analysis. This approximation is justified as long as a typical curvature of the domain wall is much smaller than the width of the domain wall, i.e.,  $R \gg m_a^{-1}$ . This condition is only marginally justified as a typical radius of the bubble is of order  $m_a^{-1}$ , which is the same order of magnitude as the width of the wall. At the same time, the width of the QCD substructure of the domain wall (including the  $\eta'$  substructure and the baryon substructure) is very small in comparison with the curvature, and it does satisfy the criteria of a thin wall approximation as  $m^{-1} \ll R \sim m_a^{-1}$ . Precisely this QCD substructure plays a crucial role in our analysis in Sec. IV where we studied the local violation of the baryon charge in the presence of the domain walls. The broad structure of the domain wall due to the axion field with the width  $m_a^{-1}$  does not play any role. However, precisely this structure determines the large tension  $\sigma \sim m_a^{-1}$  of the domain wall.

We want to effectively account for this physics by assuming that  $\sigma(R)$  effectively depends on the radius of the bubble  $R$ . On physical grounds, we expect that  $\sigma(R)$  approaches its asymptotic value at large  $R$  when the domain wall is almost flat,  $\sigma(R \rightarrow \infty) \rightarrow \sigma_0$ , while  $\sigma$  reduces its value at smaller  $R$  and eventually vanishes at some cutoff  $R_{\text{cut}}$ . A natural choice is  $R_{\text{cut}} \simeq 0.24R_0$ , which corresponds to large  $\mu_{\text{cut}} \lesssim 500$  MeV from (38), when the chemical potential assumes its typical CS value. To introduce such an infrared cutoff smoothly, it is convenient to parametrize  $\sigma$  as

$$\sigma(R) = \sigma_0 e^{-r_0/2(R-R_{\text{cut}})}, \quad (\text{B1})$$

where  $\sigma_0 \simeq 9f_a^2 m_a$  is the conventional domain wall tension, see, e.g., Ref. [10], while  $r_0$  is a free phenomenological parameter,  $0 < r_0 \lesssim R_0$ , as we expect  $\sigma(R_0) \simeq \sigma_0$ . In our numerical studies, we verified that the physical results (such as formation size  $R_{\text{form}}$ ) are not very sensitive to parameter  $r_0$ .

Another parameter which requires some comments is the viscosity  $\eta$ . In the context of the present work, the viscosity accounts for a number of different QCD effects which lead to dissipation and friction. Such effects include, but are not limited to, different scattering processes by quarks, gluons, or Nambu-Goldstone bosons in different phases. Furthermore, the annihilation processes which take place inside the bubble and which result in the production of a large number of strongly interacting quasiparticles also contribute to  $\eta$ . The viscosity can be computed from the first principles in weakly coupled quark-gluon phase [73]. However, we are more interested in the behavior of  $\eta$  below  $T_c$ . In this case, the computations [74] based on chiral perturbation theory suggest that  $\eta \sim m_\pi^3$ . This numerical value is quite reasonable in all respects and is consistent with simple dimensional arguments. It is also known that  $\eta(T)$  depends on temperature [74]. However, we neglect this dependence in our estimates which follow.

Now, we can proceed with our numerical studies. Since  $\sigma(R)$  is a function of  $R$  as explained above, we should start with a modified differential equation for  $R(t)$ :

$$\begin{aligned} \sigma(R)\ddot{R}(t) = & -\frac{2\sigma(R)}{R} - \frac{\sigma(R)\dot{R}^2}{R} + \Delta P(R) \\ & - \left(\frac{1}{2}\dot{R}^2 + 1\right) \frac{d\sigma(R)}{dR} - 4\eta \frac{\dot{R}}{R}. \end{aligned} \quad (\text{B2})$$

This equation is not identically the same as Eq. (45) discussed in Sec. VI. This is due to the fact that the tension  $\sigma(R)$  has now become an  $R$ -dependent function as we discussed above. Equation (B2) has been solved numerically using the parameters listed in Table I. The numerical values of these parameters can be obviously somewhat modified. However, the basic qualitative features presented in Sec. VI do not drastically change when the QCD parameters are varied within a reasonable parametrical region. Our numerical studies, as we discuss below, do support the analytical qualitative results presented in Sec. VI.

We start our short description with Fig. 4. It shows a typical evolution of a bubble with time. The frequencies of oscillations are determined by the axion mass  $m_a^{-1}$ , while the typical damping time is determined by parameter  $\tau$  as discussed in Sec. VI. To make the pattern of oscillations visible, the viscosity has been rescaled<sup>17</sup> At large times,  $t \rightarrow \infty$ , the solution settles at  $R_0/R_{\text{form}} \simeq 2.9$  and

<sup>17</sup>In this plot, we use  $\eta \simeq 10^8 \eta_0$ , which is 8 orders of magnitude larger than  $\eta_0 \simeq m_\pi^3$ . We did it on purpose. First, it simplifies the numerics. Indeed, the  $\eta$  parameter determines the dumping time scale (53) which is many orders of magnitude longer than any other scales of the problem. Second, we use  $\eta \simeq 10^8 \eta_0$  for demonstration purposes. Indeed, a typical oscillation time  $\omega^{-1}$  and the damping time scale  $\tau$  are characterized by drastically different scales. If we take  $\eta$  according to its proper QCD value, then the time scale in Fig. 4 would be 8 orders of magnitude longer than shown.

TABLE I. Table for some numerical parameters.

Quantity	Symbol	Value	QCD units ( $m_\pi = 1$ )
Flavors	$N_f$	2	2
Colors	$N_c$	3	3
Degeneracy factor (in) (29)	$g^{\text{in}}$	12	12
Degeneracy factor (out) (26)	$g^{\text{out}}$	37	37
Baryon charge on Domain wall (DW) (20)	$N$	2	2
Axion decay constant	$f_a$	$10^{10}$ GeV	$7 \times 10^{10}$
Mass of axion	$m_a$	$6 \times 10^{-4}$ eV	$4 \times 10^{-12}$
Domain wall tension	$\sigma_0$	$5 \times 10^8$ GeV <sup>3</sup>	$2 \times 10^{11}$
Bag constant (31)	$E_B$	$(150 \text{ MeV})^4$	1.5
Squeezer parameter (31)	$\mu_1$	330 MeV	2.4
Cosmological time scale	$t_0$	$10^{-4}$ s	$10^{19}$
Initial $\mu$	$\mu_0$	1.35 MeV	0.01
Initial radius	$R_0$	$10^{-2}$ cm	$10^{11}$
Initial temperature	$T_0$	100 MeV	0.74
QCD viscosity [74]	$\eta_0$	0.002 GeV <sup>3</sup>	1

$\mu_{\text{form}} \approx 330 \text{ MeV} \sim \mu_1$ , consistent with the qualitative analysis of Sec. VI.

We now describe Fig. 5, where we zoom in the first few oscillations of a typical solution shown in the previous plot in Fig. 4. We want to emphasize that a seeming cusp singularity is actually a smooth function near  $R_{\text{min}}$ . It looks “cuspy” as a result of a large time scale in Fig. 4. The cusp’ is relatively narrow compared to the macroscopic period of oscillation ( $\delta t_{\text{cusp}} \sim 10^{-3} R_0$ ). Nevertheless, it actually lasts much longer in comparison with a typical QCD-scale ( $\delta t_{\text{cusp}} \gg \Lambda_{\text{QCD}}^{-1}$ ).

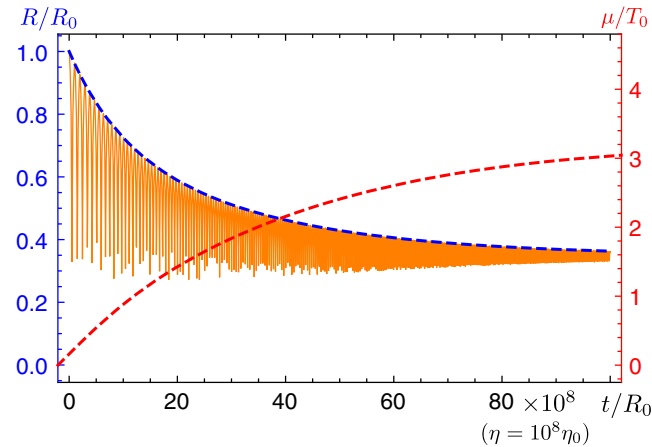


FIG. 4. Typical underdamped solution of  $R(t)$  and  $\mu(t)$ . The oscillations with frequencies  $\sim m_a^{-1}$  are shown in orange, and the modulation of  $R(t)$  is shown in blue. The chemical potential  $\mu(t)$  is shown in red. The initial  $R_0 = 10^{11}$  fm and  $r_0 = 0.5R_0$ .

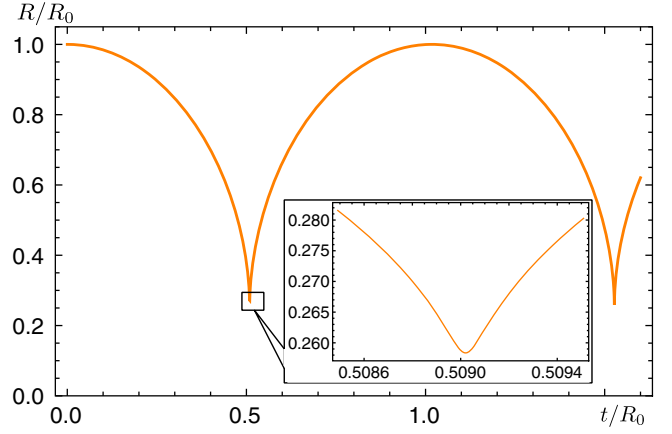


FIG. 5. The first few oscillations of an underdamped solution shown in Fig. 4.

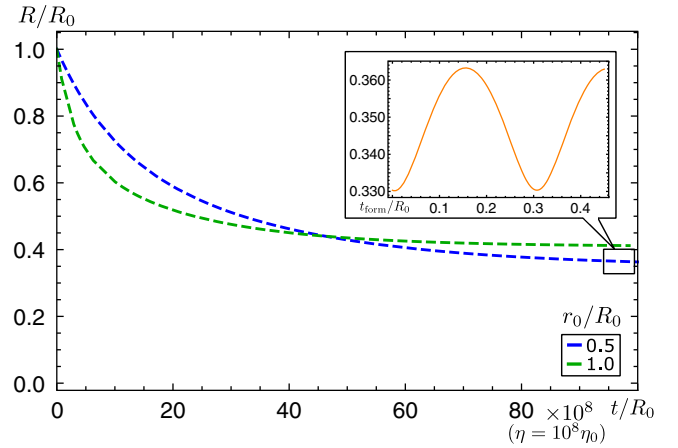
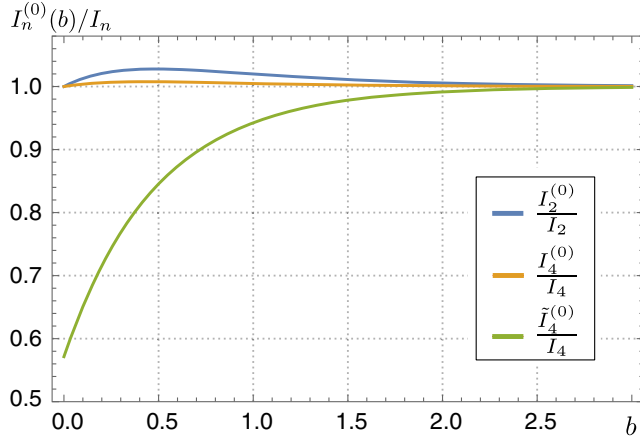


FIG. 6. Dependence on parameter  $r_0$  as defined by Eq. (B1). The zoom in shows small oscillations during the final stage of formation.

In Fig. 6, we demonstrate a (non)sensitivity of the system to parameter  $r_0$  introduced in Eq. (B1). One can explicitly see that the initial evolution is indeed quite sensitive to *ad hoc* parameter  $r_0$ . However, the final stage of the evolution is not sensitive to  $r_0$ . In other words, the physical parameters  $R_{\text{form}}$  and  $\tau$  are not sensitive to *ad hoc* parameter  $r_0$ . Note that the estimation of damping time  $\tau$  and period of oscillation  $t_{\text{osc}}$  agree well with qualitative estimations presented in Sec. VI.

### APPENDIX C: EVALUATION OF FERMİ-DİRAC INTEGRALS

The main goal of this Appendix is to present some supporting arguments to suggest that the approximation we have used in Sec. VI A and which involves the Fermi-Dirac integrals is qualitatively justified. Indeed, the relevant integrals which enter Eqs. (36) and (39) have the form


 FIG. 7. Comparison of  $I_n^{(0)}$  to  $I_n$  with different values of  $b$ .

$$I_n(b) \equiv \int_0^\infty \frac{dx \cdot x^{n-1}}{e^{x-b} + 1}, \quad b = \frac{\mu}{T} > 0, \quad (\text{C1})$$

where  $n = 2$  appears in integral (36), while  $n = 4$  appears in (39). We will hence focus on the evaluation of  $I_2$  and  $I_4$  in this Appendix. They can be exactly evaluated as

$$I_2(b) = \frac{\pi^2}{6} + \frac{1}{2}b^2 + \text{Li}_2(-e^{-b}) \quad (\text{C2a})$$

$$I_4(b) = \frac{7\pi^4}{60} + \frac{\pi^2}{2}b^2 + \frac{1}{4}b^4 + 6 \text{Li}_4(-e^{-b}), \quad (\text{C2b})$$

where  $\text{Li}_2(-z)$  and  $\text{Li}_4(-z)$  are the polylogarithm functions of orders 2 and 4, respectively. Polylogarithm functions are commonly known to represent the Fermi-Dirac and Bose-Einstein integrals. The polylogarithm functions are defined as

$$\text{Li}_n(-z) = \sum_{k=1}^{\infty} \frac{(-1)^k}{k^n} z^k. \quad (\text{C3})$$

Note that  $|z| = e^{-b} \leq 1$  for any positive  $b$ . In this case,  $\text{Li}_n(-z)$  is evidently fast converging, so we can efficiently

estimate it by extracting the leading exponent  $e^{-b}$  then use the Taylor expansion for the remaining piece,

$$\text{Li}_2(-e^{-b}) \simeq e^{-b} \left[ -\frac{\pi^2}{12} + \left( \ln 2 - \frac{\pi^2}{12} \right) b + \mathcal{O}(b^2) \right]$$

$$\text{Li}_4(-e^{-b}) \simeq e^{-b} \left[ -\frac{\pi^4}{720} + \left( \frac{3\zeta(3)}{4} - \frac{7\pi^4}{720} \right) b + \mathcal{O}(b^2) \right],$$

where  $\zeta(3) \simeq 1.202$  is the Riemann zeta function. Neglecting the terms of order  $\mathcal{O}(be^{-b})$ , which are small in both limits, at large and small chemical potentials, one can approximate  $I_2$  and  $I_4$  as follows:

$$I_2^{(0)} \simeq \frac{\pi^2}{6} + \frac{1}{2}b^2 - \frac{\pi^2}{12}e^{-b} + \mathcal{O}(be^{-b}) \quad (\text{C4a})$$

$$I_4^{(0)} \simeq \frac{7\pi^4}{60} + \frac{\pi^2}{2}b^2 + \frac{1}{4}b^4 - \frac{7\pi^4}{120}e^{-b} + \mathcal{O}(be^{-b}). \quad (\text{C4b})$$

We test our approximation by comparing our approximate expressions (C4a) and (C4b) with exact formulas (C2a) and (C2b). As one can see from Fig. 7, our approximations shown in blue ( $I_2^{(0)}/I_2$ ) and orange ( $I_4^{(0)}/I_4$ ) are very good with errors less than 3% in the entire range of  $b > 0$ .

On the same plot, we also show the approximation  $\tilde{I}_4^{(0)}$  for approximate expression  $I_4^{(0)}$  used in the main text in Eq. (39):

$$\tilde{I}_4^{(0)} \simeq \frac{7\pi^4}{60} + \frac{\pi^2}{2}b^2 + \frac{1}{4}b^4 - \frac{\pi^4}{12}e^{-b}. \quad (\text{C5})$$

The error for  $\tilde{I}_4^{(0)}$  is quite large for very small chemical potential  $b \ll 0.5$ , on the level of 40%, shown in green. The error becomes much smaller after a short period of time when  $b = \mu/T \geq 0.5$  becomes sufficiently large. To conclude, the approximations of the integrals in Sec. VIA are sufficiently good for the qualitative analysis presented in that section.

- [1] E. Witten, *Phys. Rev. D* **30**, 272 (1984).  
 [2] E. Farhi and R. Jaffe, *Phys. Rev. D* **30**, 2379 (1984); **30**, 2379 (1984); C. Alcock and E. Farhi, *Phys. Rev. D* **32**, 1273 (1985); J. Madsen, H. Heiselberg, and K. Riisager, *Phys. Rev. D* **34**, 2947 (1986); Alcock and A. Olinto, *Phys. Rev. D* **39**, 1233 (1989).  
 [3] A. R. Zhitnitsky, *J. Cosmol. Astropart. Phys.* **10** (2003) 010.  
 [4] D. H. Oaknin and A. Zhitnitsky, *Phys. Rev. D* **71**, 023519 (2005).

- [5] R. D. Peccei and H. R. Quinn, *Phys. Rev. D* **16**, 1791 (1977); S. Weinberg, *Phys. Rev. Lett.* **40**, 223 (1978); F. Wilczek, *Phys. Rev. Lett.* **40**, 279 (1978).  
 [6] J. E. Kim, *Phys. Rev. Lett.* **43**, 103 (1979); M. A. Shifman, A. I. Vainshtein, and V. I. Zakharov, *Nucl. Phys.* **B166**, 493 (1980).  
 [7] M. Dine, W. Fischler, and M. Srednicki, *Phys. Lett. B* **104**, 199 (1981); A. R. Zhitnitsky, *Yad. Fiz.* **31**, 497 (1980); *Sov. J. Nucl. Phys.* **31**, 260 (1980).

- [8] K. van Bibber and L. J. Rosenberg, *Phys. Today* **59**, 30 (2006).
- [9] S. J. Asztalos, L. J. Rosenberg, K. van Bibber, P. Sikivie, and K. Zioutas, *Annu. Rev. Nucl. Part. Sci.* **56**, 293 (2006).
- [10] P. Sikivie, arXiv:astro-ph/0610440v2.
- [11] G. G. Raffelt, *Lect. Notes Phys.* **741**, 19 (2008).
- [12] P. Sikivie, *Int. J. Mod. Phys. A* **25**, 554 (2010).
- [13] L. J. Rosenberg, *Proc. Nat. Acad. Sci.*, 112 (2015) 12278.
- [14] G. Rybka, A. Wagner, A. Brill, K. Ramos, R. Percival, and K. Patel, *Phys. Rev. D* **91**, 011701 (2015).
- [15] P. W. Graham, I. G. Irastorza, S. K. Lamoreaux, A. Lindner, and K. A. van Bibber, *Annu. Rev. Nucl. Part. Sci.* **65**, 485 (2015).
- [16] M. G. Alford, A. Schmitt, K. Rajagopal, and T. Schäfer, *Rev. Mod. Phys.* **80**, 1455 (2008).
- [17] K. Rajagopal and F. Wilczek, in *At the Frontier of Particle Physics*, edited by M. Shifman (World Scientific, 2000), Vol. 3.
- [18] A. D. Sakharov, *JETP Lett.* **5**, 24 (1967).
- [19] A. D. Dolgov, arXiv:hep-ph/9707419.
- [20] A. Zhitnitsky, *Phys. Rev. D* **74**, 043515 (2006).
- [21] D. H. Oaknin and A. R. Zhitnitsky, *Phys. Rev. Lett.* **94**, 101301 (2005).
- [22] A. Zhitnitsky, *Phys. Rev. D* **76**, 103518 (2007).
- [23] K. Lawson and A. R. Zhitnitsky, *J. Cosmol. Astropart. Phys.* **01** (2008) 022.
- [24] M. M. Forbes, K. Lawson, and A. R. Zhitnitsky, *Phys. Rev. D* **82**, 083510 (2010).
- [25] M. M. Forbes and A. R. Zhitnitsky, *J. Cosmol. Astropart. Phys.* **01** (2008) 023.
- [26] M. M. Forbes and A. R. Zhitnitsky, *Phys. Rev. D* **78**, 083505 (2008).
- [27] K. Lawson and A. R. Zhitnitsky, *Phys. Lett. B* **724**, 17 (2013).
- [28] K. Lawson, *Phys. Rev. D* **83**, 103520 (2011).
- [29] K. Lawson, *Phys. Rev. D* **88**, 043519 (2013).
- [30] K. Lawson and A. R. Zhitnitsky, *Cosmic Frontier Workshop: Snowmass 2013*, Menlo Park, California, 2013 (unpublished).
- [31] E. S. Abers, A. K. Bhatia, D. A. Dicus, W. W. Repko, D. C. Rosenbaum, and V. L. Teplitz, *Phys. Rev. D* **79**, 023513 (2009).
- [32] P. W. Gorham, *Phys. Rev. D* **86**, 123005 (2012).
- [33] P. W. Gorham and B. J. Rotter, arXiv:1507.03545.
- [34] K. Lawson and A. R. Zhitnitsky, *Phys. Lett. B* **757**, 376 (2016).
- [35] K. Lawson and A. R. Zhitnitsky, arXiv:1510.07646.
- [36] P. Sikivie, *Phys. Rev. Lett.* **48**, 1156 (1982); A. Vilenkin and A. E. Everett, *Phys. Rev. Lett.* **48**, 1867 (1982).
- [37] M. M. Forbes and A. R. Zhitnitsky, *J. High Energy Phys.* **10** (2001) 013.
- [38] D. T. Son, M. A. Stephanov, and A. R. Zhitnitsky, *Phys. Rev. Lett.* **86**, 3955 (2001).
- [39] G. Gabadadze and M. A. Shifman, *Phys. Rev. D* **62**, 114003 (2000).
- [40] T. W. B. Kibble, *J. Phys. A* **9**, 1387 (1976); W. Zurek, *Nature (London)* **317**, 505 (1985).
- [41] W. Zurek, *Phys. Rep.* **276**, 177 (1996).
- [42] A. Vilenkin and E. P. S. Shellard, *Cosmic Strings and Other Topological Defects* (Cambridge University Press, Cambridge, England, 1994).
- [43] O. Wantz and E. P. S. Shellard, *Phys. Rev. D* **82**, 123508 (2010); O. Wantz and E. P. S. Shellard, *Nucl. Phys.* **B829**, 110 (2010).
- [44] J. Preskill, M. B. Wise, and F. Wilczek, *Phys. Lett. B* **120**, 127 (1983); L. Abbott and P. Sikivie, *Phys. Lett. B* **120**, 133 (1983); M. Dine and W. Fischler, *Phys. Lett. B* **120**, 137 (1983).
- [45] S. Chang, C. Hagmann, and P. Sikivie, *Phys. Rev. D* **59**, 023505 (1998).
- [46] M. Kawasaki, K. Saikawa, and T. Sekiguchi, *Phys. Rev. D* **91**, 065014 (2015).
- [47] E. Witten, *Ann. Phys. (N.Y.)* **128**, 363 (1980).
- [48] E. Witten, *Phys. Rev. Lett.* **81**, 2862 (1998).
- [49] M. M. Forbes and A. R. Zhitnitsky, *Phys. Rev. Lett.* **85**, 5268 (2000); arXiv:hep-ph/0102158.
- [50] S. Mandelstam, *Phys. Rev. D* **11**, 3026 (1975).
- [51] S. Coleman, *Phys. Rev. D* **11**, 2088 (1975).
- [52] R. Jackiw and C. Rebbi, *Phys. Rev. D* **13**, 3398 (1976).
- [53] D. Kharzeev and A. Zhitnitsky, *Nucl. Phys.* **A797**, 67 (2007).
- [54] D. E. Kharzeev, *Ann. Phys. (Amsterdam)* **325**, 205 (2010).
- [55] D. E. Kharzeev, *Prog. Part. Nucl. Phys.* **75**, 133 (2014).
- [56] D. E. Kharzeev, J. Liao, S. A. Voloshin, and G. Wang, *Prog. Part. Nucl. Phys.* **88**, 1 (2016).
- [57] I. E. Halperin and A. Zhitnitsky, *Phys. Rev. Lett.* **81**, 4071 (1998).
- [58] T. Fugleberg, I. E. Halperin, and A. Zhitnitsky, *Phys. Rev. D* **59**, 074023 (1999).
- [59] T. Hiramatsu, M. Kawasaki, K. Saikawa, and T. Sekiguchi, *Phys. Rev. D* **85**, 105020 (2012); **86**, 089902(E) (2012).
- [60] C. Beck, *Phys. Rev. Lett.* **111**, 231801 (2013).
- [61] C. Beck, *Phys. Dark Univ.* **7–8**, 6 (2015).
- [62] C. Hoffmann, F. Lefloch, M. Sanquer, and B. Pannetier, *Phys. Rev. B* **70**, 180503(R) (2004).
- [63] T. E. Golikova, F. Hübler, D. Beckmann, I. E. Batov, T. Yu. Karminskaya, M. Yu. Kupriyanov, A. A. Golubov, and V. V. Ryazanov, *Phys. Rev. B* **86**, 064416 (2012).
- [64] L. He *et al.*, arxiv:1107.0061.
- [65] M. H. Bae, R. C. Dinsmore III, M. Sahu, H.-J. Lee, and A. Bezryadin, *Phys. Rev. B* **77**, 144501 (2008).
- [66] M. A. Metlitski and A. R. Zhitnitsky, *Nucl. Phys.* **B731**, 309 (2005).
- [67] A. Parnachev and A. R. Zhitnitsky, *Phys. Rev. D* **78**, 125002 (2008).
- [68] A. R. Zhitnitsky, *Nucl. Phys.* **A813**, 279 (2008).
- [69] M. D’Elia and F. Negro, *Phys. Rev. D* **88**, 034503 (2013).
- [70] C. Bonati, M. D’Elia, H. Panagopoulos, and E. Vicari, *Phys. Rev. Lett.* **110**, 252003 (2013).
- [71] C. Bonati, *J. High Energy Phys.* **03** (2015) 006.
- [72] C. Bonati, M. D’Elia, and A. Scapellato, *Phys. Rev. D* **93**, 025028 (2016).
- [73] P. B. Arnold, G. D. Moore, and L. G. Yaffe, *J. High Energy Phys.* **11** (2000) 001.
- [74] J.-W. Chen and E. Nakano, *Phys. Lett. B* **647**, 371 (2007).